Cerebral Cortex, December 2017;27: 5444–5462

doi: 10.1093/cercor/bhw311
Advance Access Publication Date: 14 October 2016
Original Article

ORIGINAL ARTICLE

Highly Dynamic Spatiotemporal Organization of Low-Frequency Activities During Behavioral States in the Mouse Cerebral Cortex

Laura M. J. Fernandez[1,2], Jean-Christophe Comte[2,3,4], Pierre Le Merre[1,2], Jian-Sheng Lin[1,2], Paul-A. Salin[2,3,4], and Sylvain Crochet[1,2,5]

[1]INSERM U1028, CNRS UMR5292, Lyon Neuroscience Research Center, Integrative Physiology of the Brain Arousal System Team, Lyon Cedex 08 F-69000, France, [2]Lyon Neuroscience Research Center, University Lyon 1, Lyon Cedex 08 F-69000, France, [3]INSERM U1028, CNRS UMR5292, Lyon Neuroscience Research Center, Forgetting and Cortical Dynamics Team, Lyon Cedex 08 F-69000, France, [4]INSERM U1028, CNRS UMR5292, Lyon Neuroscience Research Center, Biphoton Microscopy, Lyon F-69000, France, and [5]Current address: Laboratory of Sensory Processing, EPFL, Lausanne CH-1015, Switzerland

Address correspondence to Sylvain Crochet, Laboratory of Sensory Processing, Faculty of Life Science, Brain Mind Institute, SV-BMI-LSENS, Station 19, Ecole Polytechnique Fédérale de Lausanne (EPFL), CH-1015 Lausanne, Switzerland. Email: sylvain.crochet@epfl.ch

Abstract

Although low-frequency (LF < 10 Hz) activities have been considered as a hallmark of nonrapid eye movement (NREM) sleep, several studies have recently reported LF activities in the membrane potential of cortical neurons from different areas in awake mice. However, little is known about the spatiotemporal organization of LF activities across cortical areas during wakefulness and to what extent it differs during NREM sleep. We have thus investigated the dynamics of LF activities across cortical areas in awake and sleeping mice using chronic simultaneous local field potential recordings. We found that LF activities had higher amplitude in somatosensory and motor areas during quiet wakefulness and decreased in most areas during active wakefulness, resulting in a global state change that was overall correlated with motor activity. However, we also observed transient desynchronization of cortical states between areas, indicating a more local state regulation. During NREM sleep, LF activities had higher amplitude in all areas but slow-wave activity was only poorly correlated across cortical areas. Despite a maximal amplitude during NREM sleep, the coherence of LF activities between areas that are not directly connected dropped from wakefulness to NREM sleep, potentially reflecting a breakdown of long-range cortical integration associated with loss of consciousness.

Key words: cortical dynamics, local field potential, long-range synchrony, NREM sleep, wakefulness

Introduction

Mammalian brain constantly adapts to internal and external conditions. One of the most obvious sign of this adaptation is the change in brain electrical activity that can easily be recorded using scalp electroencephalography (EEG), which samples the summated activity of thousands of neurons. Since the pioneer works of Berger (1929), this technique has been extensively used to study cortical activities in relation to behavioral states in humans and different animal species (Loomis et al. 1935; Rheinberger and Jasper 1937; Moruzzi and Magoun 1949; Jouvet 1967; Steriade et al. 1993a; Hobson and Pace-Schott 2002). Based on these EEG studies, wakefulness has been classically

described as a state of global neocortical "desynchronization" dominated by low-voltage, high-frequency (HF > 20 Hz) electrical activities, whereas nonrapid eye movement (NREM) sleep has been described as a state of global neocortical "synchronization" dominated by high-voltage, low-frequency (LF < 10 Hz) activities (Lin 2000; Steriade 2000; Hobson and Pace-Schott 2002; Jones 2005; Brown et al. 2012). Later on, it was found that HF cortical activities during wakefulness can be highly synchronous within and across cortical areas; therefore, the terms "activated" and "deactivated" were proposed to replace the terms "desynchronized" and "synchronized," respectively (Steriade et al. 1996; Destexhe et al. 1999; Steriade 2000). In rodents, the cortical EEG conventionally recorded between the frontal and parietal cortices or the parietal cortex and the cerebellum, also shows prominent theta activity (5–10 Hz) during wakefulness (Maloney et al. 1997; Franken et al. 1998; Parmentier et al. 2002), which may result from the diffusion of the theta oscillation generated in the hippocampus due to volume conduction (Sirota et al. 2008). The EEG samples a very large region of the cortex and may therefore not always faithfully reflect the local neuronal activity.

Recent studies using local extracellular or intracellular recording approaches have revealed a modulation of cortical activities during wakefulness in the rodent cortex which is not as clearly observed with cortical EEG. LF, high-amplitude cortical activities have been reported in different cortical areas of awake rodents, including the primary somatosensory (Crochet and Petersen 2006; Okun et al. 2010; Reimer et al. 2014; Zhao et al. 2016), visual (Bennett et al. 2013; Polack et al. 2013; Reimer et al. 2014), and auditory (Schneider et al. 2014; Zhou et al. 2014) areas, the primary motor area (Zagha et al. 2013), as well as the medial prefrontal cortex (mPFC; Okun et al. 2010; Fujisawa and Buzsaki 2011; Parker et al. 2014; Karalis et al. 2016). In particular, recent studies by our team and others have correlated the membrane potential of cortical neurons in the awake mouse with motor activity (whisker movements or locomotion). These studies have revealed complex cortical dynamics in the primary sensory areas with a clear state change related to motor activity (Crochet and Petersen 2006; Bennett et al. 2013; Polack et al. 2013; Reimer et al. 2014; Schneider et al. 2014; Zhou et al. 2014; Zhao et al. 2016). This state change occurs as a transition from LF, high-amplitude (10–20 mV) membrane potential fluctuations that are highly synchronous between nearby neurons when the mouse is quiet, to low-amplitude, fast, and desynchronized membrane potential fluctuations at slightly more depolarized level during periods of motor activity (Poulet and Petersen 2008; Gentet et al. 2010; Zhao et al. 2016).

However, to date little is known about the spatiotemporal organization of LF activities across cortical areas during wakefulness and to what extent LF activities are different during wakefulness and NREM sleep. To answer these questions, we have performed simultaneous local field potential (LFP) recordings from 5 to 6 targeted brain regions in chronically implanted head-fixed mice during wakefulness and NREM sleep. LF neuronal activities and state change can faithfully be reported using LFP (Poulet and Petersen 2008; Poulet et al. 2012). The cortical activity was correlated to the overall motor activity that was monitored by recording nuchal electromyogram (EMG). LFPs were targeted to sensorimotor cortical areas that are densely interconnected—the primary and secondary somatosensory areas (S1, and S2) and the primary motor area (M1) (Aronoff et al. 2010; Zingg et al. 2014; Suter and Shepherd 2015)—as well as sensory areas from different modalities—the primary visual (V1) and auditory (Au1) areas. We also targeted associative and higher order cortical areas which are not directly, or weakly, connected with the sensorimotor areas (Zingg et al. 2014): we recorded from the parietal associative area (PtA), the mPFC, and the CA1 area of the dorsal hippocampus (dCA1).

Our study first confirmed the prominence of LF activities in most cortical areas during quiet wakefulness and a global cortical activation (i.e. low LF/HF ratio) during active wakefulness, but we also found regional specificities, with a stronger expression of LF activities during quiet wakefulness, and a more pronounced state change during active wakefulness, in somatosensory, and motor areas (S1, S2, and M1). The mPFC showed a prominent and narrow band LF (2-6 Hz) oscillatory activity during quiet wakefulness, which slightly increased in frequency during active wakefulness. We also observed transient desynchronization of cortical states between cortical areas, with spatially restricted occurrence of LF activities and activation. During NREM sleep, LF activities increased in all cortical areas compared with wakefulness. However, we found that the amount of slow-wave activity (SWA) (0.25–2 Hz), a marker of slow-wave sleep, fluctuated in each cortical area with overall little synchrony between cortical areas. Also surprising, despite the general increase in LF activities during NREM sleep, the interareal coherence in this frequency domain strongly decreased compared with wakefulness, except for areas that are strongly coupled via direct corticocortical connections (S1, S2, and M1). Interestingly, the highest levels of coherence in the LF range were found during active wakefulness, with very strong coherences between mPFC or PtA and the other cortical areas. Our results thus reveal an important and fast reorganization of long-range functional connectivity in the LF domain consistent with a state of high cortical integration during active wakefulness and a breakdown of cortical integration correlated with loss of consciousness during NREM sleep.

Materials and Methods

Animal Preparation

All procedures were approved by the University of Lyon 1 Animal Care Committee (project DR2013-4) and were conducted in accordance with the French and European Community guidelines for the use of research animals. All efforts were made to minimize the number of animals used and their suffering. Eighteen adult male C57BL/6 mice (Janvier SAS, St. Berthevin, France; 6–8 weeks old at the time of surgery) were anesthetized with isoflurane supplemented with a mixture of N_2O and O_2. Carprofene (subcutaneously, 5 mg/kg) was administered during the surgery. Subcutaneous injections of saline (0.10–0.15 mL NaCl 0.9%) were administered every hour during the surgery to prevent dehydration. A heating blanket maintained the rectally measured body temperature at 37°C. The head of the mouse was fixed in a stereotaxic apparatus (Kopf) using ear-bars. The skin overlying the cortex was removed and the bone gently cleaned. Five to six high-impedance sharp tungsten microelectrodes (10–12 MΩ, 75 µm shaft diameter, from Frederick Haer & Co., FHC, United States of America) were stereotaxically implanted individually using interaural coordinates (Paxinos and Franklin 2008). The recording sites included the barrel field of the primary somatosensory cortex (S1; AP 2.8, lat 3.2, depth from surface 0.5); the secondary somatosensory cortex (S2; AP 3.1, lat 4.0, depth from surface 0.8); the primary motor area (M1; AP 5.1, lat 1.8, depth from surface 0.4); the primary auditory cortex (Au1; AP 1.3, lat 4.0, depth from surface 0.6); the primary visual cortex (V1; AP 0.5, lat 2.5, depth from surface 0.4); the PtA (AP 1.8, lat 1.8, depth from surface 0.4); the prelimbic area of the mPFC (AP 5.7, lat 0.3, depth from surface 1.85), and the dCA1 (AP 1.3, lat 2.0, depth from surface 1.3). Small

craniotomies (~300 μm in diameter) were performed to allow the insertion of each electrode that was slowly lowered vertically to the recording depth. For neocortical areas, the tip of the electrode was lowered to a depth of 300–400 μm from the pia. For hippocampus, we targeted the stratum radiatum of dCA1. When in position, the electrodes were glued to the skull (Cyanoacrylate adhesive, Sigma Aldrich) and cemented using acrylate dental cement (Palavit). Each electrode was then soldered to a small electric connector. In addition, 2 conventional surface EEG electrodes were implanted onto the duramater over the parietal (AP 2.0, lat 1.5) and frontal areas (AP 5.3, lat 1.5) of the contralateral hemisphere. Two electrodes were inserted in the neck muscles for nuchal EMG recordings. Two silver wires were inserted on both sides of the cerebellum for reference and grounding. A light-weight metal head-post was also cemented to the skull allowing painless head-fixation during recording sessions (Crochet 2012). At the end of the recording sessions, the animals were deeply anesthetized with pentobarbital (60 mg/kg; intraperitoneally). Small electrolytic lesions were performed to localize the position of each electrode. The animal was then transcardially perfused with 4% paraformaldehyde (PFA). The brain was removed and postfixed in 4% PFA. Brain sections of 100 μm were cut to identify the recording sites.

Habituation and Recordings

After 3–5 days of recovery from surgery, the mice were progressively habituated to head-restrain conditions, with habituation sessions gradually increasing from 10–30 min to 2–3 h. At the end of each session, the mice were rewarded with few drops of sweet water. Recording sessions started after 1–2 weeks of habituation, when the first NREM sleep episodes were observed. The mice were housed in their home cage on 12 h light/dark cycle (light-on at 7 AM) with water and food being available at libitum and ambient temperature maintained at 22 ± 2°C. Recordings were performed during the light period (between 12 AM and 5 PM) in an electrically shielded recording chamber, at same ambient temperature (22 ± 2°C) in semidark light condition. Each electrode was connected to the head-stage of the amplifier (custom modified Model 3000 AC/DC Differential Amplifiers, A-M Systems, United States of America). LFPs were recorded using 1 of the 2 silver wires implanted in the cerebellum as reference, the other wire being connected to the ground. EEG and EMG were recorded differentially. Signals were band-pass filtered between 0.1, and 1000 Hz for the LFPs and EEG, and 10, and 20 000 Hz for the EMG. The signals were digitalized and recorded at 1 kHz on a Vision XP (LDS Nicolet). To estimate a possible contamination of the LFP by the EMG, in 4 mice we recorded broadband (0.1–20 000 Hz) LFPs and EMG signals during wakefulness. For those recordings, the signals were digitalized and recorded at 2 kHz.

In half of the mice (n = 9), we performed simultaneous recordings of the LFP and EMG with high-speed video filming of the whisker movements. To facilitate whisker tracking, all the whiskers except the C2 whisker were trimmed on both sides under light isoflurane anesthesia. After full recovery (2–3 h), the mouse was positioned on the set-up for recording. Whisker movements were filmed at 200 fps. Electrophysiological recordings and video synchronization were performed using an ITC-18 analog-to-digital converter under the control of IgorPro. Thirty seconds long epochs were recorded and filmed during the session. A custom written routine (from C. Matéo, Laboratory of Sensory Processing, EPFL, Lausanne) running under IgorPro was used to automatically track the whisker position offline.

Database

Simultaneous LFP activities were recorded in 18 awake head-restrained mice from 5, or 6 of the following cortical areas: the whisker field of the primary (S1, n = 17) and secondary (S2, n = 9) somatosensory areas; the primary visual (V1, n = 8) and auditory (Au1, n = 8) areas; the primary motor cortex (M1, n = 8); the PtA (n = 8); the prelimbic area of the mPFC (n = 11); and dCA1 (n = 17). In 8 mice we targeted S1, S2, M1, mPFC, and dCA1. In 6 mice, we targeted S1, Au1, V1, PtA, mPFC, and dCA1. In 2 mice, we targeted S1, S2, PtA, mPFC, dCA1, and Au1, and in 2 other mice we targeted S1, S2, PtA, mPFC, dCA1, and V1. The recordings used for analysis were selected based on histological verification and the absence of artifacts. Six sites out of 100 could not be verified by histology but have been included in the analysis based on the location of the other sites in the same mouse and the similarity of recorded activity compared with identified sites in other mice.

Data Analysis and Statistics

Data analysis was performed using custom written routines under IgorPro (Wavemetrics) and Matlab (MathWorks). The recordings were first examined by visual inspection to extract periods of wakefulness and NREM sleep based on standard scoring using EEG and EMG (Valatx 1971; Franken et al. 1998; Parmentier et al. 2002; Takahashi et al. 2006). Wakefulness was defined by high and phasic EMG activity and low 1–5 Hz EEG activity, that contrasted with periods of NREM sleep defined by low and regular EMG activity and high 1–5 Hz EEG activity. Transition periods of drowsiness and intermediate sleep, as well as episodes of rapid-eye movement sleep were discarded, so that the epochs of wakefulness and NREM sleep selected for analysis showed a clear separation (see Supplementary Fig. 1). All the epochs of wakefulness or NREM sleep from the different recording sessions of a same mouse were then pooled together for analysis. The total duration of the selected epochs of wakefulness and NREM sleep used for analysis varied depending on each mouse tendency to fall asleep during the recording session. On average, the total recording duration analyzed was 2689 ± 820 s for wakefulness and 1641 ± 745 s for NREM sleep (mean ± SD).

To extract the amplitude envelop of the LF activities of the LFPs, we first band-pass filtered the LFPs (1–10 Hz), then extracted the instantaneous amplitude using Hilbert transform. The instantaneous amplitude was low-pass filtered (0–1 Hz) to extract the LF envelop. The variability of the LF amplitude was assessed as the coefficient of variation (CV) of the LF amplitude envelop. To assess possible multistates, we computed the bimodality coefficient (b) of the distribution of the LF amplitude envelop using the estimation for a finite sample:

$$b = \frac{g^2 + 1}{k + \frac{3(n+1)^2}{(n-2)(n-3)}}$$

where b is the bimodality coefficient, g is the sample skewness, k is the sample excess kurtosis, and n is the sample size. b reaches a maximum value of 1.0 for a perfect bimodal distribution and has a value of 0.333 for a unimodal Gaussian distribution.

In previous studies, we have used whisker movements to assess the behavior of the mouse (Crochet and Petersen 2006; Poulet and Petersen 2008; Gentet et al. 2010). However, high-speed video filming is not adapted to long, continuous recording. We therefore used instead nuchal EMG recording to assess

the overall motor activity. In 9 mice, we verified that the nuchal EMG is a good estimator of motor activity by simultaneously filming the whisker movements and recording the EMG (Fig. 1A). To directly compare the EMG and whisker movements, we measured the correlation between the standard deviation (σ) of the whisker position and the logarithm of the σ of the EMG (Fig. 1B). For every mouse, we found a strong and significant correlation between whisker movements and EMG activity. Thus, the nuchal EMG is a good indicator to assess overall motor activity and can be used to classify quiet and active periods of wakefulness.

The classification as quiet and active wakefulness was performed automatically. The instantaneous EMG amplitude was computed using a Hilbert transform that was low-pass filtered (0–10 Hz). A threshold was applied to score periods of low or high EMG activity. Consecutive periods of low activity were merged if separated by less than 30 ms of high EMG activity. Consecutive periods of high EMG activity were merged if separated by less than 500 ms of low EMG activity. Four seconds time windows were then classified as quiet wakefulness or active wakefulness if the EMG activity was scored as low or high, respectively, during the entire time window after merging process.

In many mammal species, NREM sleep can be subclassified in different stages from light NREM sleep occurring just after transition from drowsiness to NREM sleep and characterized by high sleep spindle activity (10–15 Hz), to deep NREM sleep characterized by high-SWA (0.25–2 Hz) (Steriade et al. 1991; Aeschbach and Borbely 1993; Steriade and Amzica 1998; Gervasoni et al. 2004). In rodents, however, this classification is

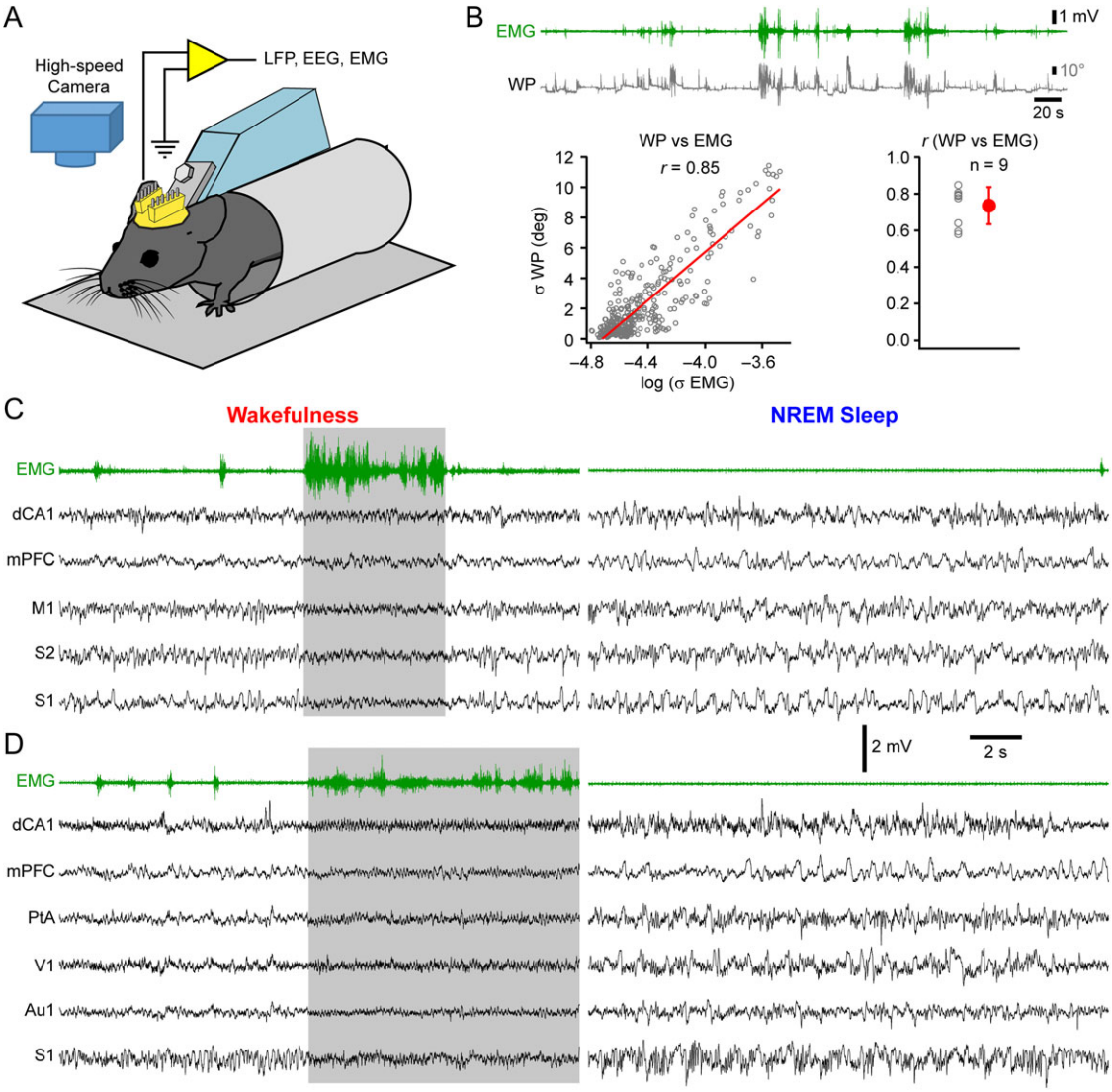

Figure 1. Multisite LFP recording and behavioral monitoring. (*A*) Schematic drawing of the experimental configuration. (*B*) *Top*, example of nuchal EMG recording (green trace) and whisker angular position (WP, gray; protraction upward) extracted from simultaneous high-speed video filming. *Bottom-left*, whisker movements (σ WP) and EMG activity (log σ EMG) computed for 2 s time-windows from the example recording above were highly correlated (Pearson correlation coefficient, $r = 0.85$; *t* statistics, $P = 1.02e{-}108$). *Bottom-right*, in all simultaneous whisker filming and EMG recording, we found a high and significant correlation between whisker movements and EMG activity ($n = 9$ mice, linear correlation with *t* statistics, $P < 1e{-}43$; $r = 0.74 \pm 0.10$, mean ± SD). (*C*) Example of a simultaneous recording of EMG and LFPs from dCA1, mPFC, M1, S2, and S1 from the same mouse during active (gray shading) and quiet wakefulness and NREM sleep. (*D*) Example of simultaneous recording of EMG and LFPs from dCA1, mPFC, PtA, V1, Au1, and S1 from another mouse. LFPs in panels C and D were band-pass filtered between 0.25 and 100 Hz.

more difficult and light and deep NREM sleep appear more as a continuum with increasing amount of SWA (Gervasoni et al. 2004). We thus subclassified NREM sleep epochs according to the amount SWA. For each LFP, we quantified the amount of SWA as the mean amplitude of the Fast Fourier Transform (FFT) in the slow (0.25–2 Hz) frequency band using 4 s sliding windows with steps of 2 s. The SWA was z-scored for each LFP and a global SWA index was computed as the average of the z-scored SWA computed for each LFP recorded from a given mouse. Four seconds time windows of NREM sleep epochs were then subclassified as low- and high-SWA if they belong to the lower (0–25%) or higher (75–100%) quartile of the distribution of the global SWA index.

Spectral analysis was performed on raw LFP recordings by computing the FFT amplitude using a Hamming window for 4 s time-windows for each recording site and each behavioral state (active wakefulness, quiet wakefulness, and NREM sleep). The FFT mean amplitude for the LF band (1–10 Hz) and the LF over HF ratio were computed on single 2, or 4 s time-window FFTs. The LF/HF ratio was computed as the ratio of the mean FFT amplitudes in the LF (1–10 Hz) and HF (30–90 Hz) bands, respectively. FFTs, mean FFT amplitudes, and LF/HF ratios were averaged for each mouse, recording site, and behavioral state. Grand averages were computed by averaging individual averages across the population.

Interareal correlation of cortical states during wakefulness was assessed by computing the LF/HF ratio for each LFP as the ratio between the LFP amplitude in the LF band and the amplitude in the HF band using Hilbert transform after band-pass filtering (1–10 Hz for LF and 30–90 Hz for HF). Cross-correlograms of the LF/HF ratio were computed for each pair of recording sites in each mouse. The correlation was taken as the peak amplitude of each correlogram and was averaged across mice.

To evaluate the synchronization of cortical activities across areas, we computed the mean coherence between each recording site in the different behavioral states and then averaged across mice. The coherence in a given frequency band was taken as the mean coherence within this frequency band. To compute the mean coherence between 2 cortical areas for a given state of vigilance (active wakefulness, quiet wakefulness, and NREM sleep), we first concatenated all the epochs corresponding to this state. The coherence was then computed using 4 s time windows as the cross-power spectra of the 2 signals using the following formula:

$$\gamma^2_{XY}(f) = \frac{|\overline{X(f)Y^*(f)}|^2}{|\overline{X(f)}|^2|\overline{Y(f)}|^2}$$

where $X(f)$ and $Y(f)$ are the Fourier transform of the 2 signals $x(t)$ and $y(t)$ coming from 2 different areas, while the sign star corresponds to the complex conjugate. The mean of the cross-spectra between $X(f)$ and $Y(f)$ (numerator) is normalized by the total variability in the frequency domain (denominator). To estimate the noise level in our coherence measurements, we also computed the coherence between LFPs for each mouse and behavioral state after shuffling the 4 s time windows between LFPs. In 4 mice, we also assessed the coherence between the broadband recorded LFPs and EMG during wakefulness.

The correlation between whisker movements and EMG activity was assessed using parametric Pearson correlation with t statistic. For all the other comparisons, we used non-parametric statistical tests. Comparisons between states were done using Wilcoxon signed-rank test with Bonferroni correction when more than 2 states were compared. Multiple comparison between cortical areas was done using Kruskal–Wallis test followed by Dunn–Holland–Wolfe test. The correlation between LFP LF/HF ratio and EMG activity was assessed using Spearman rank correlation test and a Fisher z-transformation was applied to the Spearman rank correlation coefficient (Rs) before performing a Kruskal–Wallis test followed by Dunn–Holland–Wolfe test to compare correlations between areas.

Results

LF Cortical Activities in the Awake and Sleeping Mouse

To assess the expression of LF activities across cortical areas and behavioral states, we performed simultaneous LFP recordings from 5 to 6 cortical areas in awake and sleeping head-fixed mice (Fig. 1A). Using different configurations of electrode implantations, we recorded several close and distant areas in sensory cortices (S1, S2, V1, and Au1), motor cortex (M1) and associative and higher order cortices (PtA, mPFC, and dCA1). To correlate cortical activities with the mouse overall motor activity, we recorded the nuchal EMG. In 9 mice, we performed simultaneous LFP and EMG recording and high-speed video filming of whisker movements. We found that EMG activity was well correlated with whisker movements and therefore could be used to monitor the mice behavior (Fig. 1B). Each mouse was recorded over several 2–3 h recording sessions during which they spontaneously went through periods of quiet and active wakefulness and periods of NREM sleep showing different patterns of cortical activities (Fig. 1C and D). We specifically quantified LF activities in the LFPs by computing the instantaneous amplitude of the band-pass filtered (1–10 Hz) LFPs using Hilbert transform (Fig. 2A). We observed that the mean and distribution of the amplitude of LF activities varied across behavioral states and cortical areas (Fig. 2B). Compared with wakefulness, the amplitude of LF activities increased significantly in all cortical areas during NREM sleep (Fig. 2C, top). LF activities showed less variability (lower CV) during NREM sleep in most sensory and motor areas but higher variability in PtA and mPFC (Fig. 2D, top). Across areas, LF activities had highest amplitude in S1, and S2, both during wakefulness and NREM sleep (Fig. 2C, bottom). The variability of LF activities was the highest in S1, S2, M1, and V1 during wakefulness and in mPFC during NREM sleep (Fig. 2D, bottom). During wakefulness, we observed a clear tendency toward bimodal distribution of the amplitude of LF activities in some areas (Fig. 2B). We thus computed the bimodality coefficient of the distribution of amplitude (see Materials and Methods) for each recording site and state of vigilance. During NREM sleep, the bimodality coefficient was close to that of a unimodal Gaussian distribution (0.33) for most areas, whereas during wakefulness, the bimodality coefficient was significantly higher for S1, S2, M1, and V1 (Fig. 2E). Thus, overall, LF activities had lower amplitude but appeared more variable over time and across cortical areas during wakefulness than during NREM sleep.

The bimodal distribution of the amplitude of LF activities in S1, S2, M1, and V1 during wakefulness reflects certainly state changes occurring during quiet and active wakefulness in these areas (Crochet and Petersen 2006; Bennett et al. 2013; Polack et al. 2013; Zagha et al. 2013; Reimer et al. 2014). To define more precisely to what extent cortical activities changed across areas and behavioral states, we subclassified the recordings during wakefulness according to EMG activity, as active wakefulness and quiet wakefulness, and computed the averaged FFTs for each state (Fig. 3 and see Supplementary Fig. 2). Although LF

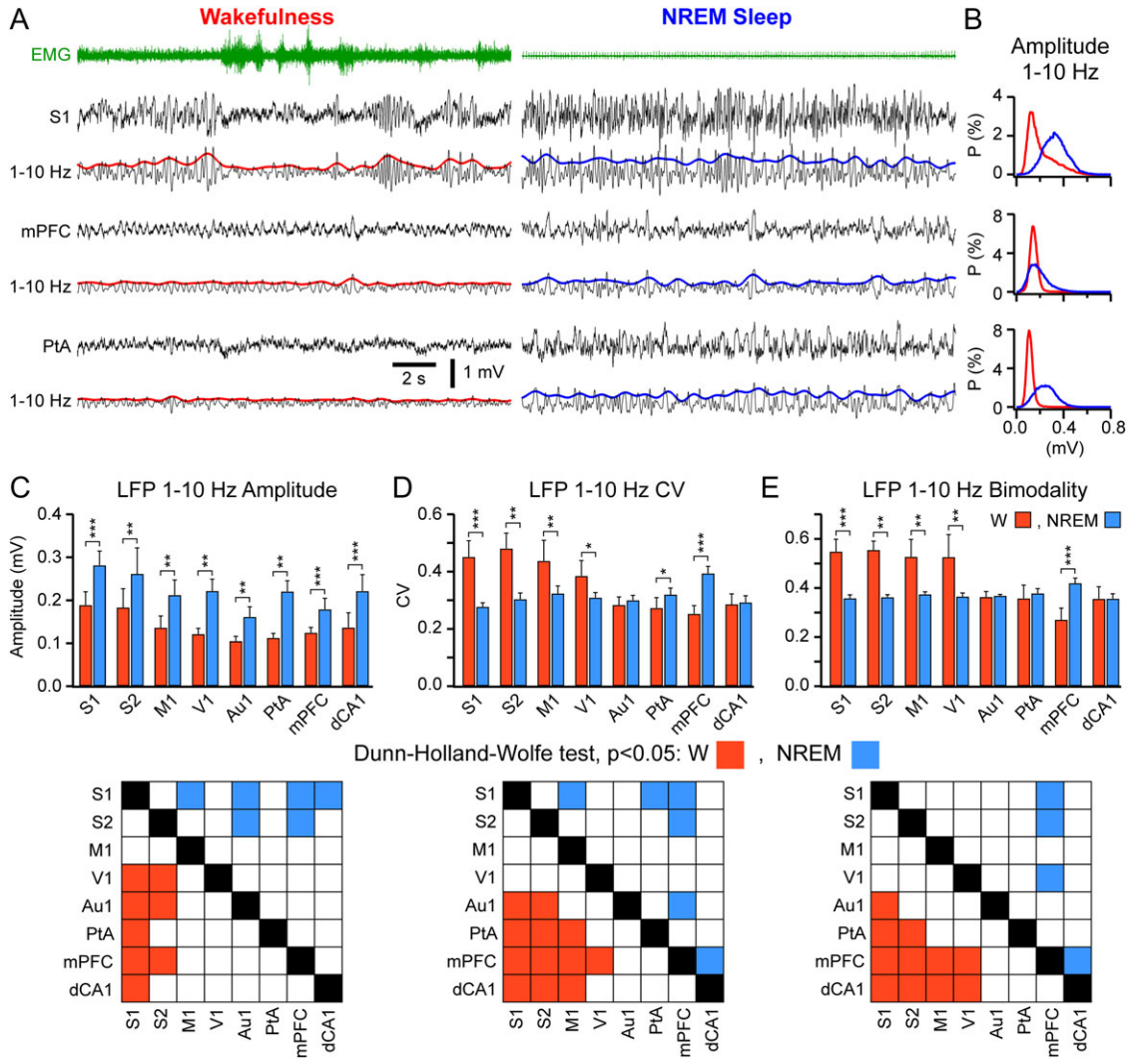

Figure 2. Differential expression of LF activities during wakefulness and NREM sleep across cortical areas. (*A*) An example of simultaneous recording of EMG (green trace) and LFPs from S1, mPFC, and PtA during wakefulness (W) and NREM sleep (NREM) from the same mouse. The raw LFPs (upper traces) were band-pass filtered in the LF band (1–10 Hz, lower traces) and the amplitude of LF activities was extracted using Hilbert transform (plain thick lines, red for W, and blue for NREM). (*B*) Normalized histograms showing the distribution (probability, *P*) of the amplitude of LF activities for all W (red) and NREM (blue) epochs from the mouse shown in panel *A*. The amplitude of LF activities had different distribution across cortical areas and states of vigilance. (*C*) Mean amplitude of LF activities for each area and state (blue, NREM; red, W). Quantified across the population, LF cortical activity had significantly higher mean amplitude during NREM than during W in all cortical areas (*Top panel*). LF activities had higher amplitude in S1, and S2 compared with the other areas, especially during wakefulness (*Bottom panel*). (*D*) The variability of LF activities was measured as the CV of the amplitude. The CV of LF activities amplitude was higher during W than during NREM in S1, S2, M1, and V1, and was lower during W than during NREM in PtA and mPFC (*Top panel*). Overall, the CV of the amplitude of LF activities was more homogeneous across cortical areas during NREM than during W (*Bottom panel*). (*E*) The bimodality coefficient of the distribution of LF activities amplitude was computed for each area and state of vigilance. S1, S2, M1, and V1 had a more bimodal distribution during W than during NREM (*Top panel*). During NREM, the bimodality coefficient was more homogeneous across areas and closer to the bimodality coefficient of a Gaussian distribution (0.33) (*Bottom panel*). Values are mean ± SD. Statistical comparisons between W and NREM were assessed with Wilcoxon signed-rank test: $^{*}P < 0.05$; $^{**}P < 0.01$; $^{***}P < 0.001$; and $P > 0.05$ when not indicated. Statistical comparisons between areas were assessed using Kruskal–Wallis test followed by Dunn–Holland–Wolfe, $P < 0.05$.

activities dominated all states, LF increased from active to quiet wakefulness in all areas, except for the mPFC (Fig. 3*B* and see Supplementary Fig. 3). LF activities during quiet wakefulness occurred as a broadband irregular activity in most areas (Fig. 3*A* and see Supplementary Fig. 4). In the mPFC, however, a clear oscillatory activity with narrower frequency band (2–6 Hz) was very prominent during quiet wakefulness and could persist with a slightly higher peak frequency during active wakefulness (Fig. 3*A* and see Supplementary Fig. 4). Theta activity clearly dominated hippocampal (dCA1) activity during active wakefulness and persisted during quiet wakefulness, but with additional lower frequency activity (Figs1, and 3*A* and see Supplementary Fig. 4). Overall, the oscillatory activity in mPFC had a lower peak frequency than that in dCA1; however, during some epochs of active wakefulness, the oscillatory activity in mPFC could transiently shift toward the theta frequency of the hippocampus (see Supplementary Fig. 4). During NREM sleep, LF activities increased in all cortical areas in a broad frequency band with a peak frequency between 0.5 and 1 Hz reflecting SWA (Fig. 3*A* and see Supplementary Fig. 3). We also observed a marked increase in the alpha frequency band (10–15 Hz) reflecting sleep spindle activity. Interestingly, gamma activity (30–90 Hz) did not decrease during NREM sleep compared with quiet wakefulness in most cortical areas except the mPFC (see Supplementary

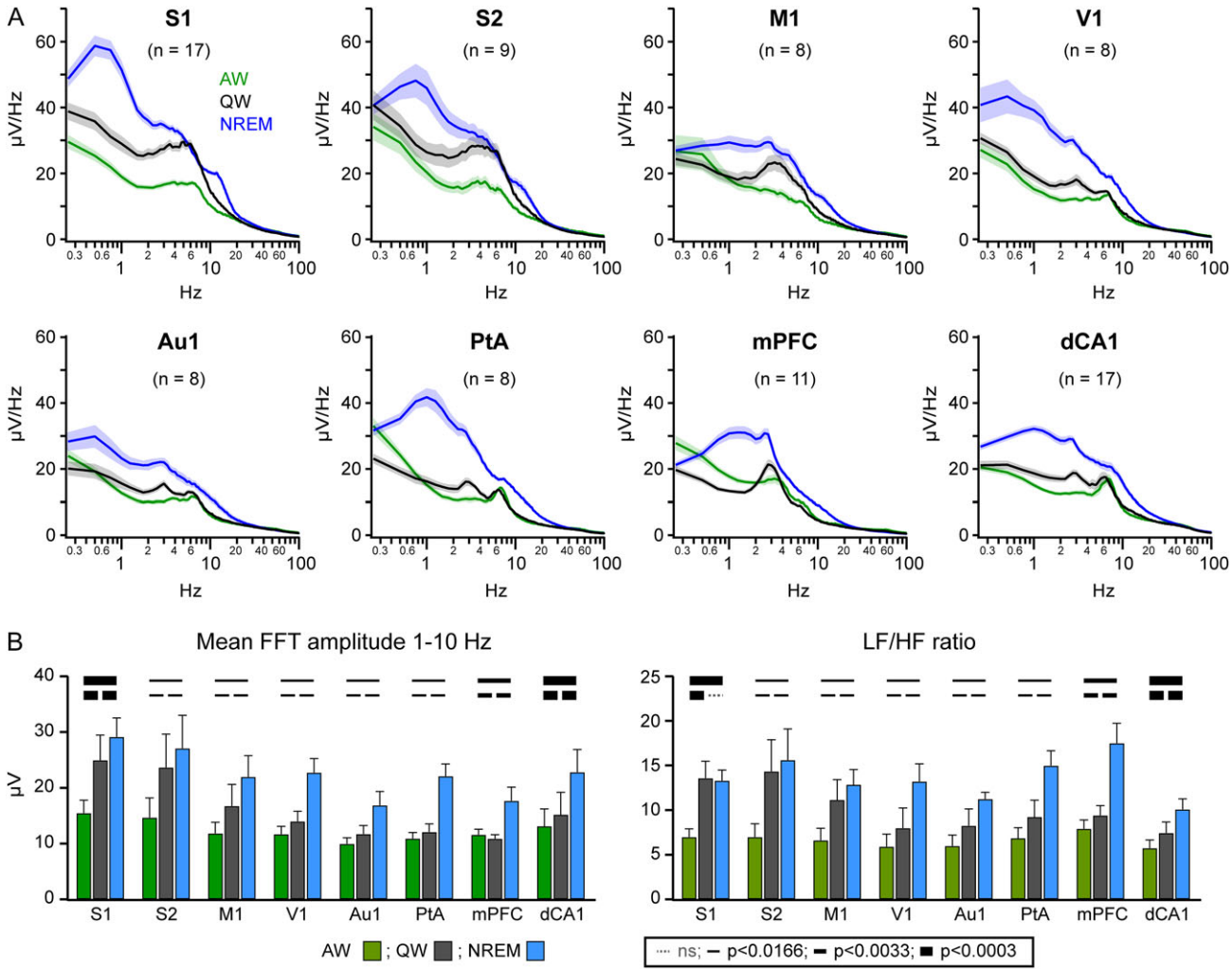

Figure 3. LFP spectral analysis during quiet and active wakefulness and NREM sleep. (*A*) Grand-average FFTs across the population for each recording site (the number of mouse is indicated in parentheses). FFTs were computed for 4 s time windows from all the epochs of quiet (QW, black) and active (AW, green) wakefulness and NREM sleep (NREM, blue). Shaded areas indicate SEM. (*B*) The mean amplitude of the FFT in the LF band (1–10 Hz) (*left panel*) and the ratio of LF over HF (30–90 Hz) (*right panel*) were computed across the population for each recording site and behavioral state. Values are mean ± SD. *P*-values were computed using Wilcoxon signed-rank test with Bonferroni correction: dashed line, nonsignificant; thin plain line, $P < 0.016$; plain line, $P < 0.003$; thick plain line, $P < 0.0003$.

Fig. 3), in good agreement with previous studies showing high gamma activity during the active phase (or up-state) of the slow-oscillation under anesthesia or natural NREM sleep (Steriade et al. 1996; Isomura et al. 2006; Mukovski et al. 2007; Mena-Segovia et al. 2008; Le Van Quyen et al. 2010).

State Change Across Cortical Areas During Wakefulness

In some areas, LF activities increased only moderately (or even decreased in mPFC) during quiet wakefulness compared with active wakefulness. However, the ratio between LF and HF activity increased significantly in all areas (Fig. 3*B*). We thus used the LF/HF ratio as a measure of local cortical activation to investigate the dynamic of the state change across cortical areas during wakefulness (Fig. 4)—a low LF/HF ratio indicating cortical activation and a high LF/HF ratio indicating cortical deactivation. We first investigated the correlation between the state change in each area and the motor activity. We computed the LF/HF ratio and motor activity (log σ EMG) for consecutive 2 s time windows. Plotting the LF/HF ratio against the EMG activity for S1, or S2 revealed a nonlinear relationship with a wide distribution of LF/HF ratio for low motor activity and a narrower distribution in the lower range of the LF/HF ratio for high motor activity (Fig. 4*B*). This result confirms recent studies indicating that activated cortical state (i.e. low LF/HF ratio) is dominant during active wakefulness, but that both activated and deactivated states can be observed during quiet wakefulness (Reimer et al. 2014; Urbain et al. 2015; Vinck et al. 2015; McGinley et al. 2015a). We used nonparametric Spearman correlation to evaluate the link between cortical and motor activity. We found a significant negative correlation between the LF/HF ratio and motor activity for all cortical areas, confirming that overall, high motor activity correlates with cortical activation in all cortical areas (Fig. 4*C*). However, we also found differences between cortical areas, with LF activities being significantly more correlated to motor activity in S1, and S2 than in mPFC, V1, and dCA1 (Kruskal–Wallis test followed by Dunn–Holland–Wolfe test after Fisher z-transformation of Spearman rank correlation coefficient, $P < 0.05$). This latter observation led us to investigate the synchronization of cortical states across areas. We thus directly

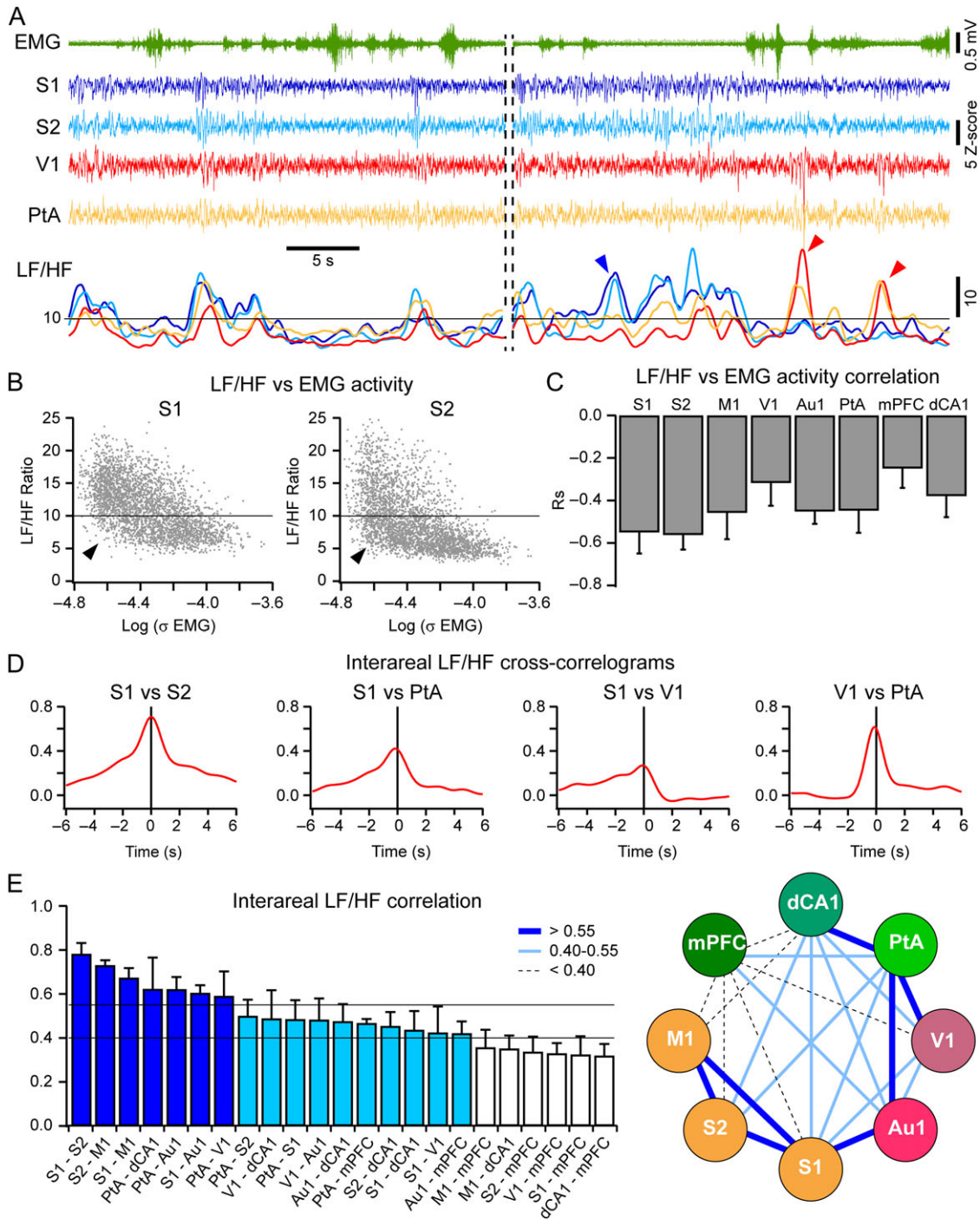

Figure 4. Cortical state change across areas during wakefulness. (*A*) Example EMG (green trace) and LFP recording from S1, S2, V1, and PtA (*top*) and corresponding LF (1–10 Hz) over HF (30–90 Hz) ratio (*bottom*, LF/HF, same color coding). Two epochs of wakefulness from the same mouse are shown. LFPs were band-pass filtered (1–100 Hz) and normalized in amplitude (z-score). The blue arrow-head indicates a period of deactivation in S1, and S2, and activation in V1, and PtA; red arrow-heads indicate periods of activation in S1, and S2, and deactivation in V1, and PtA. (*B*) LF/HF ratio vs EMG activity (Log σ EMG) for S1, and S2 (same mouse as panel A, all wakefulness epochs, each point is a 2 s time window). The black arrow-heads indicate epochs of cortical activation (low LF/HF ratio) during quiet W (low EMG activity). (*C*) Mean Spearman rank correlation coefficient (*Rs*) between LF/HF ratio and EMG activity for all the recording sites across the population. (*D*) Example cross-correlograms of LF/HF ratio between cortical areas (same mouse as panel A). (*E*) *Left*, mean peak cross-correlation of LF/HF ratio between cortical areas across the population. *Right*, connectivity diagram showing the mean interareal peak cross-correlation of LF/HF ratio. Line color and thickness indicate mean correlation range as indicated in the left histogram. Values are mean ± SD.

computed the cross-correlation of the instantaneous LF/HF ratio (Fig. 4A) between pairs of simultaneously recorded areas (Fig. 4D). We found consistent differences between pairs across the population, with some areas showing strong synchronization of the brain states and others showings only moderate synchronization (Fig. 4E). Strong synchronizations were observed between the areas S1, S2, and M1, between PtA, and dCA1, V1, and Au1, and between S1, and Au1. Lowest synchronizations were found

between mPFC and the other areas (Fig. 4E). Thus, although cortical states were overall synchronized across cortical areas (Fig. 4A, left panel), transient desynchronization did occur. The right panel of Figure 4A shows a typical example of cortical state desynchronization with S1, and S2 being deactivated while V1, and PtA are activated (blue arrow-head) or V1, and PtA showing high LF activity while S1, and S2 are activated (red arrow-heads). These episodes of transient cortical state desynchronization occurred typically during quiet wakefulness.

SWA Across Areas During NREM Sleep

Although NREM sleep appeared to be a more homogeneous state compared with wakefulness, we observed variable expression of SWA (0.25–2 Hz) across time and areas during NREM sleep (Fig. 5A). We therefore investigated whether SWA varied synchronously across areas or locally. We computed the normalized SWA amplitude for each recording site (Fig. 5B) and measured the correlation between simultaneously recorded areas (Fig. 5C). We found that overall SWA fluctuations were only poorly synchronized across areas, with periods of high SWA occurring at different times (Fig. 5A and B). The level of correlation between areas also varied across pairs: the strongest correlations of SWA were found between associative and high-order areas (mPFC, PtA, and dCA1) and between somatosensory and motor areas (S1, S2, and M1); the lowest levels of correlation were found between somatosensory and associative areas (Fig. 5D). Thus, although NREM sleep is often regarded as a state of highly synchronous cortical activity, the expression of SWA indicates a more local regulation of cortical activities during NREM sleep.

Long-Range Synchrony of LF Activities Across Behavioral States

We found that the LF activities varied in amplitude across cortical areas and behavioral states, with an overall increase in LF activities from active wakefulness to quiet wakefulness and from quiet wakefulness to NREM sleep. We next used coherence analysis to investigate how LF activities organized between cortical areas across behavioral states (Fig. 6A). We first verified to what extend the coherence between LFPs could be contaminated by EMG activity. In 4 mice, we recorded the LFPs and EMG broadband (0.1–20, 000 Hz) during wakefulness and computed the coherence between LFPs and between the LFPs and EMG (see Supplementary Fig. 5). We found that the level of coherence between the LFPs and EMG was very low (<0.025) and close to chance level (see in Fig 6B the coherence from shuffled LFP data) between1, and 70 Hz and had only minor impact (<0.07) below 1 Hz or above 70 Hz (see Supplementary Fig. 5). When computing coherence from shuffled LFP data, we also observed a nonspecific increase in the mean coherence below 0.5 Hz (Fig 6B). We thus focused our quantitative analysis of the LFP coherence between 0.5 and 70 Hz. We computed the mean coherence between pairs of simultaneously recorded LFPs for active wakefulness, quiet wakefulness, and NREM sleep (Fig. 6A and see Supplementary Fig. 6). The grand-average coherence computed across all mice and recording pairs revealed a high interareal coherence in the LF band during active and quiet wakefulness with 2 distinct peaks in the delta (2–5 Hz) and theta (5–10 Hz) frequency bands, respectively (Fig. 6B). Surprisingly, a strong decrease in the coherence in the LF band was observed during NREM sleep (Fig. 6B). We also observed a specific decrease in the coherence in a narrow gamma band around 60 Hz during NREM sleep, compared with active and quiet wakefulness.

When considering the changes in mean coherence in the LF band (0.5–10 Hz) for specific pairs, we could identify 3 groups: in the first group, the coherence decreased from active to quiet wakefulness but increased from quiet wakefulness to NREM sleep (Fig. 6C, red); in the second group, the coherence changed only moderately from active to quiet wakefulness but decreased strongly from quiet wakefulness to NREM sleep (Fig. 6C, yellow); in the last group on the contrary, the coherence decreased strongly from active to quiet wakefulness but only moderately from quiet wakefulness to NREM sleep (Fig. 6C, gray). Interestingly, this classification did not yield to any random pattern of connections but in fact revealed a clear organization of the cortical areas (Fig. 6D): the areas showing persistent or even increased coherence in the LF band during NREM sleep as compared with quiet wakefulness are the somatosensory and motor areas (S1, S2, and M1) that are strongly interconnected (Fig. 7A, B, S-M). The other areas (V1, Au1, PtA, mPFC, and dCA1) maintained a high level of coherence in the LF band during quiet wakefulness, but the coherence dropped during NREM sleep (Fig. 7A, B, not S-M). The coherence between these 2 groups dropped already during quiet wakefulness as compared with active wakefulness (Fig. 7A,B, S-M to not S-M). Thus, when going from active wakefulness to quiet wakefulness and then to NREM sleep, we observed a progressive functional disconnection of distant cortical areas that affects first the link between sensorimotor areas (S1, S2, and M1) and the other areas, then all the areas that are not directly synaptically connected (Figs 6D and 7). The same analysis for the gamma band around the peak of coherence during wakefulness (52–62 Hz) did not reveal any particular pattern of connectivity (Fig. 6C), but interestingly, the coherence in this frequency band was overall maintained during quiet wakefulness and dropped during NREM sleep for all cortical areas, including sensorimotor areas (Fig. 7). This result suggests that long-range cortical coherence in the gamma band is a good general marker of wakefulness.

As SWA varies during NREM sleep (see Fig. 5) and could significantly impact the functional connectivity between cortical areas, we investigated whether the overall level of cortical SWA had any significant impact on interareal LFP coherence. We thus selected NREM sleep epochs with low- or high- SWA (see Materials and Methods) and compared the cortical activity to that of quiet wakefulness. The cortical activity during NREM sleep epochs with low-SWA differed clearly from that recorded during quiet wakefulness, with a particular increase in amplitude in the alpha (10–15 Hz) frequency band in agreement with high spindle activity during light NREM sleep. During epochs of NREM sleep with high-SWA, a marked increase in amplitude was observed in the slow (0.25–2 Hz) frequency band in all cortical areas, but little or no difference was observed between low-SWA and high-SWA epochs in the other frequency bands (see Supplementary Fig. 7). We then compared the interareal coherence computed for quiet wakefulness, NREM sleep, and epochs of high-SWA (see Supplementary Fig. 8). We observed slightly higher levels of coherence during high-SWA epochs compared with NREM sleep throughout the LF bands and across all cortical areas. However, despite these higher levels of coherence, the coherence in the LF bands during high-SWA epochs was still significantly lower than that of quiet wakefulness for the nonsomatosensory or motor areas (not S-M areas) and between the somatosensory or motor areas and the other areas (S-M to not S-M areas), thus confirming the overall drop

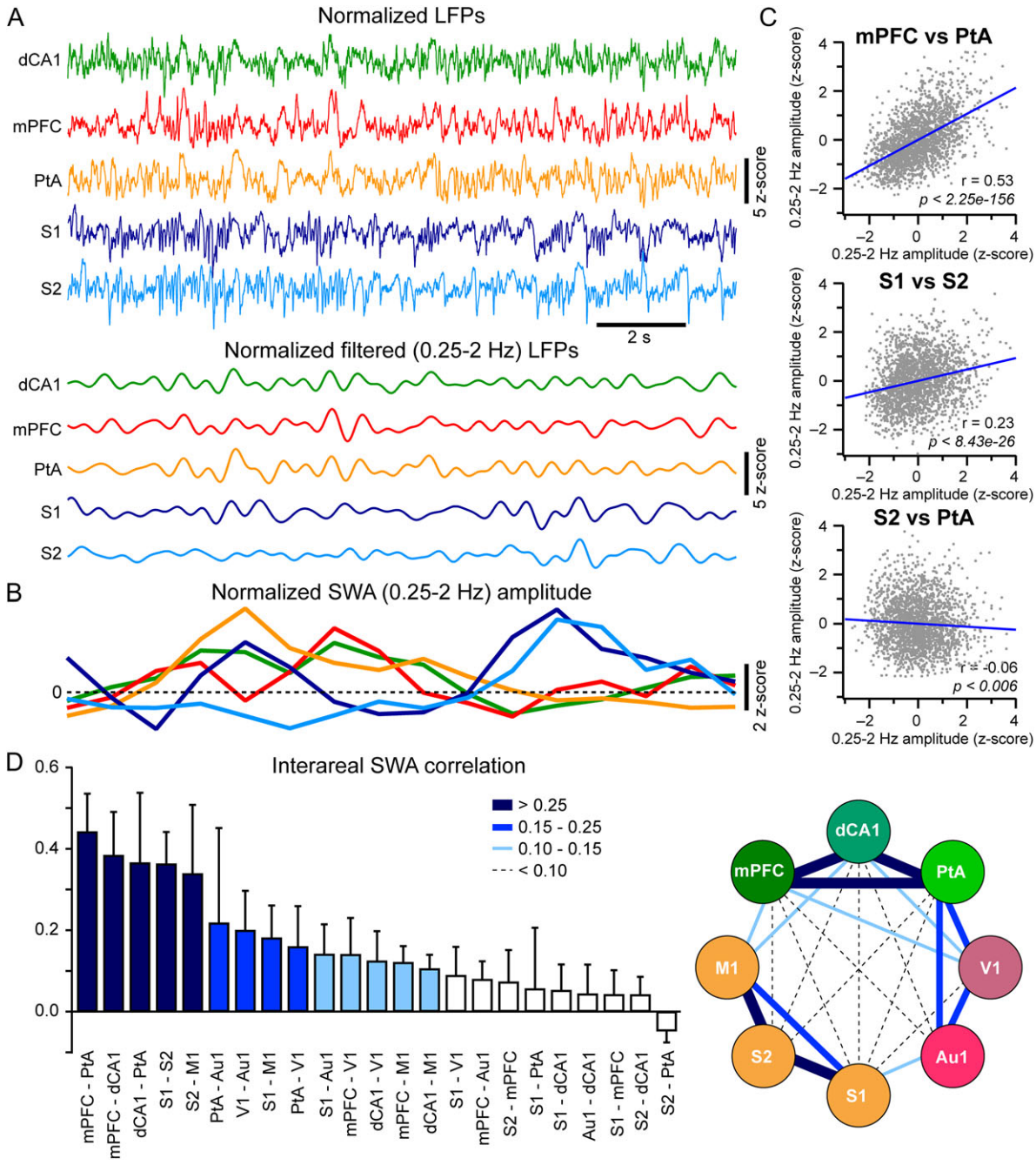

Figure 5. Asynchronous variations of SWA across cortical areas during NREM sleep. (*A*) *Top*, normalized broadband filtered (0.25–100 Hz) LFPs recorded simultaneously during NREM sleep from dCA1, mPFC, PtA, S1, and S2. *Bottom*, the same LFPs were filtered in the slow-frequency band (0.25–2 Hz) and normalized (z-score). (*B*) Normalized SWA computed as the mean amplitude of the FFT (4 s sliding windows, 1 s steps) in the slow-frequency band (0.25–2 Hz) for each LFP and z-scored. Same color code as panel *A*. (*C*) example interareal correlation of SWA with linear regression (blue line). (*D*) *Left*, mean SWA correlation between cortical areas. *Right*, connectivity diagram showing the mean interareal SWA correlation. Line color and thickness indicate mean correlation range as indicated in the left histogram. Values are mean ± SD.

of coherence in the LF bands during NREM sleep between areas that are not directly connected, regardless of the SWA.

Modulation of Interareal Coherence Across Cortical Areas

We then investigated the coherence between specific pairs of cortical areas. Figure 8 shows connectivity graphs built from the mean coherence between cortical areas for each frequency band of interest (slow 0.5–2 Hz; delta 2–5 Hz; theta 5–10 Hz; gamma peak 52–62 Hz) and each behavioral state (active wakefulness, quiet wakefulness, and NREM sleep). These connectivity graphs reveal that some areas appeared to be more strongly connected to others (Fig. 8A). Overall, we found consistently high levels of coherence between PtA and mPFC and between PtA and dCA1 in all frequency bands during wakefulness. A high level of coherence persisted during NREM sleep between PtA and mPFC in the slow-frequency band and between PtA

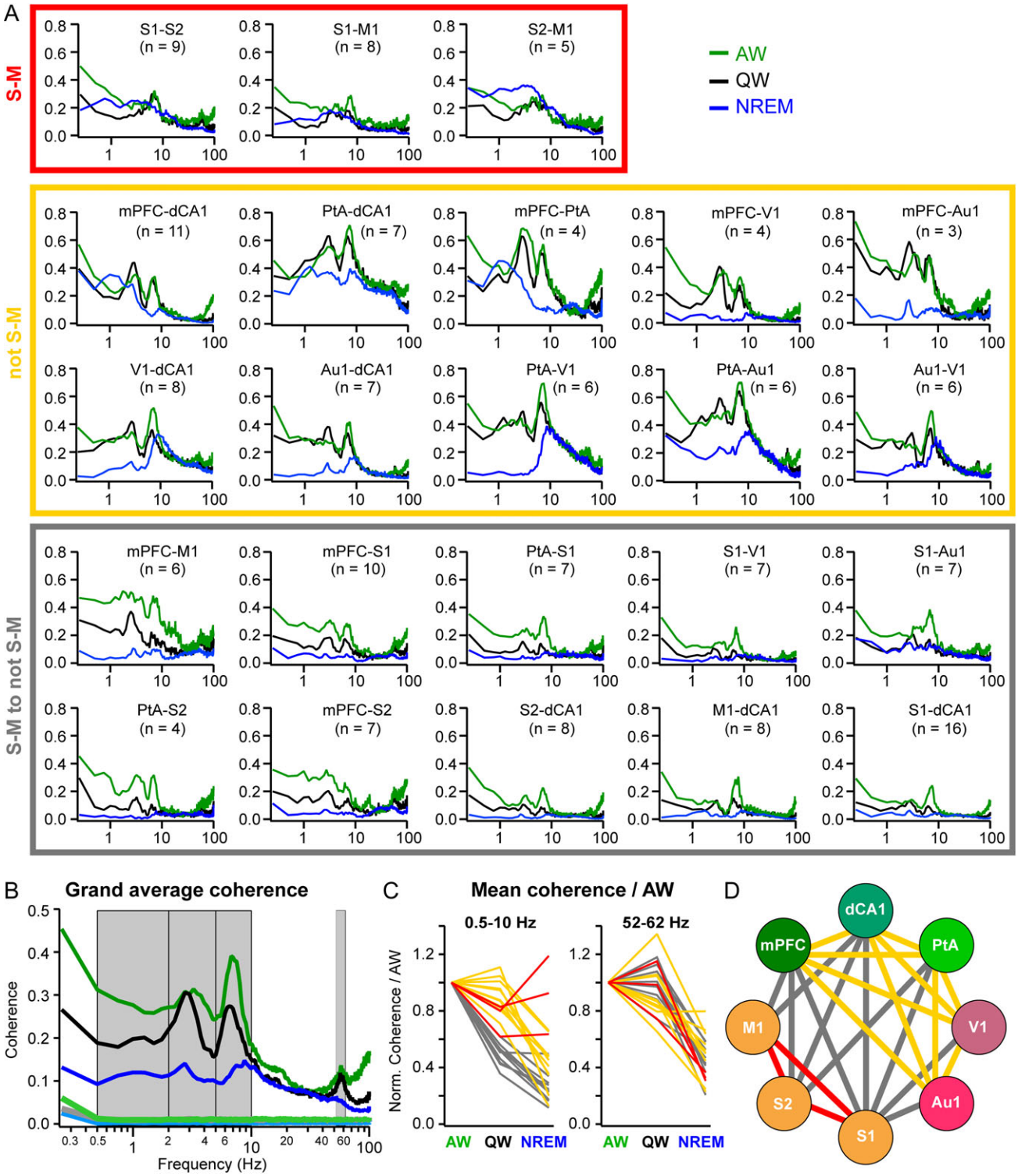

Figure 6. State-dependent change in interareal coherence. (*A*) Average interareal LFP coherences computed for each pair of simultaneously recorded cortical areas and each behavioral state across the population: green, active wakefulness (AW); black, quiet wakefulness (QW) and blue, NREM sleep (NREM). The number of mouse is indicated in parentheses for each average. The pairs of cortical areas are grouped according to color coding in panels *C* and *D*: S-M, somatosensory, and motor areas (red); not S-M, all areas except somatosensory and motor areas (yellow); S-M to not S-M, coherence between somatosensory or motor areas and all the other areas (gray). (*B*) Grand-average coherences across mice and recording pairs (green, AW; black, QW, and blue, NREM). Grand-average coherences were also computed after shuffling of the LFPs for each behavioral state: light-green, AW; gray, QW, and light-blue, NREM. Gray areas indicate the frequency bands for quantification in panel *C*. Black frames indicate the frequency bands for quantification in Figure 7. (*C*) Mean coherence computed across the population for each pair of cortical areas for the LF (0.5–10 Hz) and gamma peak (52–62 Hz) frequency bands and normalized to AW. Color coding indicates 3 groups of paired areas with different changes in coherence in the LF band relative to AW: in red, group with a decrease of the mean coherence during QW, but increase from QW to NREM; in yellow, group with moderate change during QW, but a marked decrease from QW to NREM; in gray, group with a decrease of the mean coherence larger from AW to QW than from QW to NREM. Same color coding is applied to the 52–62 Hz frequency band. (*D*) Connectivity diagram using the color coding of panel *C*.

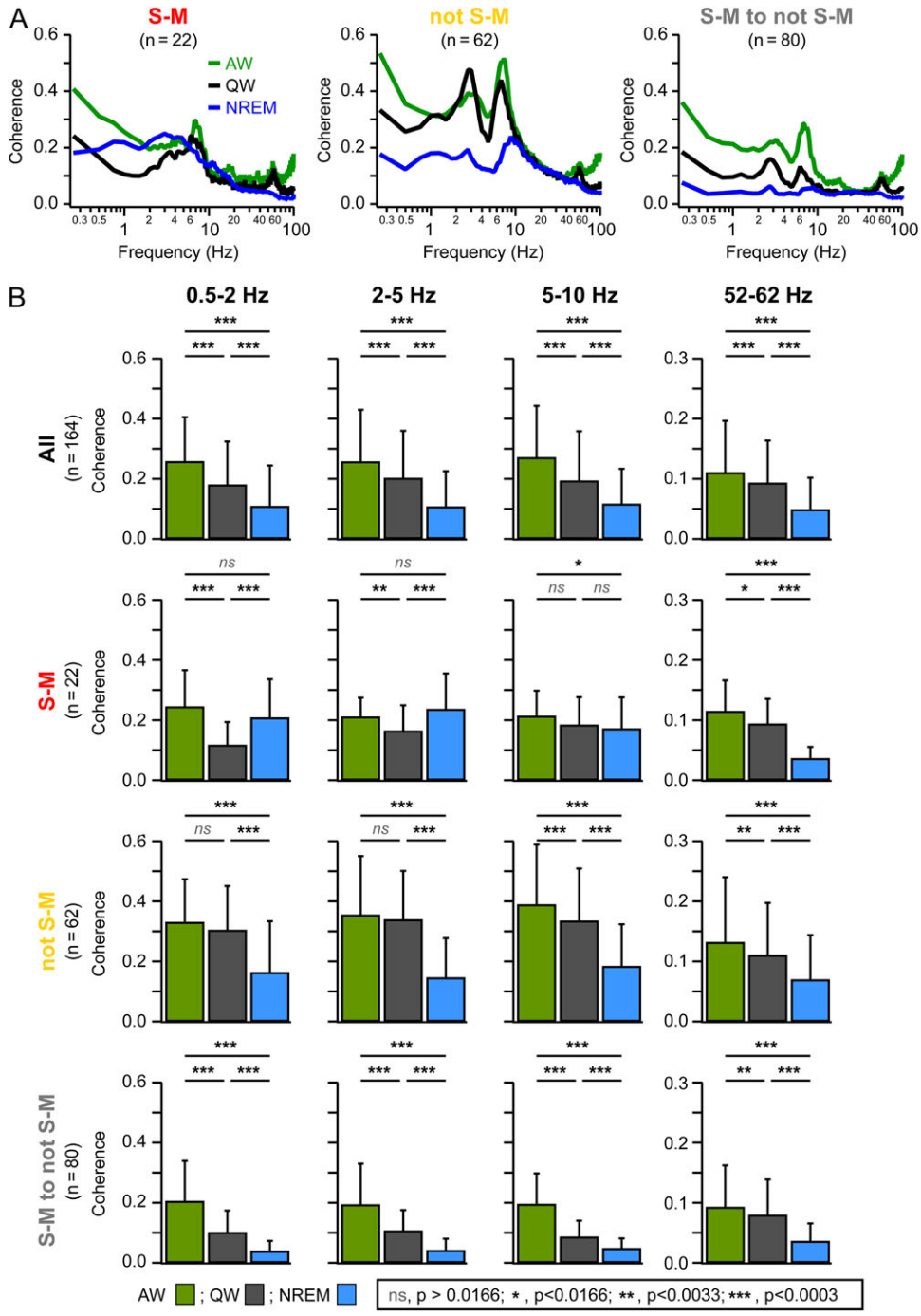

Figure 7. Area dependent change in coherence across behavioral states. (*A*) Grand-average coherences computed for the 3 groups of cortical sites: S-M, somatosensory and motor areas; not S-M, all areas except somatosensory and motor areas; S-M to not S-M, coherence between somatosensory or motor areas and all the other areas. (*B*) Comparison of the mean coherence for 4 frequency bands across behavioral states (green, AW; dark-gray, QW and blue, NREM) and groups of cortical sites (all, all cortical areas; S-M; not S-M and S-M to not S-M). The LF band was further subdivided into slow (0.5–2 Hz), delta (2–5 Hz), and theta (5–10 Hz) frequency bands (black frames in Fig. 6B). Values are mean ± SD. Comparisons between states (AW, QW, and NREM) were performed using Wilcoxon signed-rank test with Bonferroni correction: ns, nonsignificant; *P < 0.0166; **P < 0.0033; ***P < 0.0003. The total number of individual pair for each group is indicated in parentheses.

and dCA1 in the Gamma peak frequency band. During active wakefulness, PtA had the highest mean coherence with all the other areas in all frequency bands (Fig. 8B). To a lesser extent, we also found a strong coherence in the slow and delta frequency bands between mPFC and several sensory, motor, and associative areas suggesting that LF activities may play a major role in increasing the functional connectivity for close and distant cortical areas during active wakefulness (Fig. 8). Together, these results point to an important functional reorganization of long-range cortical connections in the LF domain across behavioral states and are consistent with a decreased functional coupling between cortical areas during NREM sleep. These results are also in line with the idea that some cortical areas like PtA and mPFC are more widely

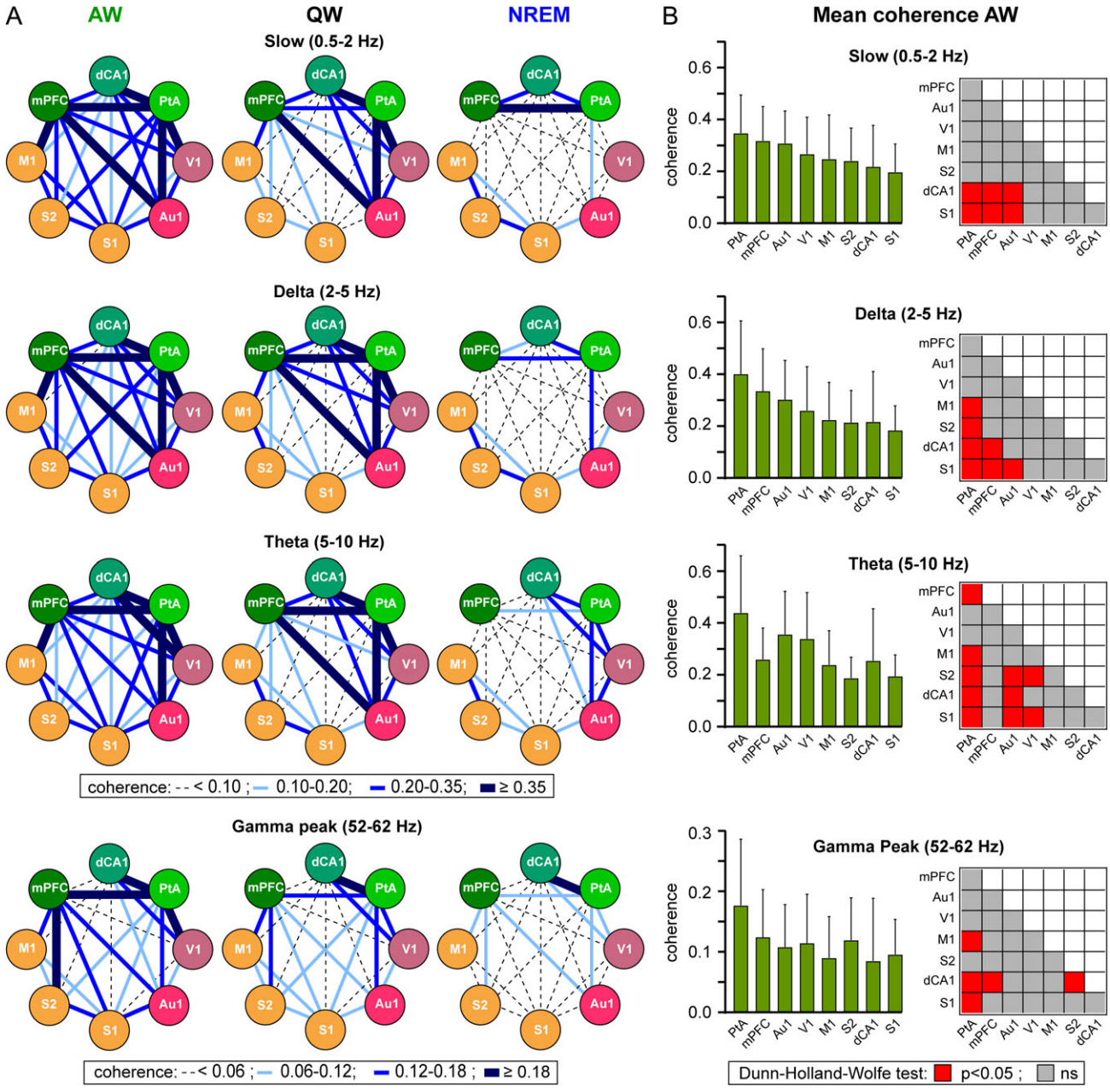

Figure 8. Interareal connectivity across behavioral states. (*A*) Connectivity diagrams showing the mean amplitude of the coherence between different areas across the population. The mean coherence was computed for AW (*left*), QW (*middle*), and NREM (*right*) in the slow (0.5–2 Hz), delta (2–5 Hz), theta (5–10 Hz), and gamma peak (52–62 Hz) frequency bands. Color coding and line thickness represent the range of mean coherence as indicated in the insets. (*B*) *Left*, recording pairs were grouped to compute the average coherence between one cortical site and all the other sites for AW in the 4 frequency bands. *Right*, the comparison of the average coherence across sites was assessed using Kruskal–Wallis test followed by Dunn–Holland–Wolfe test (red, $P < 0.05$; gray, nonsignificant, ns).

connected to other cortical areas than others and may serve as functional hubs to orchestrate cortical activities and large-scale information processing.

Discussion

We have investigated the expression of LF activities in active and quiet wakefulness compared with NREM sleep in several cortical areas of the mouse using multisite LFP recordings in combination with EEG and EMG. We found that in most cortical areas, LF activities increased in amplitude from active to quiet wakefulness and increased further from quiet wakefulness to NREM sleep. Important differences between areas were observed, particularly during wakefulness, with somatosensory and motor areas (S1, S2, and M1) showing the highest amplitude and variability in the LF band and with mPFC showing a clear narrow-band 2–6 Hz oscillation. We also confirmed and extended previous results from ours and other teams, showing a general state change from quiet to active wakefulness that was accompanied by an average decrease in LF activities in different sensory areas and a pronounced decrease in LF/HF ratio in all areas. Using LF/HF ratio as an index of cortical activation,

we found that the state changes between cortical areas were highly synchronized in the somatosensory and motor areas compared with the other areas. Transient desynchronizations of cortical states between distant areas were observed during quiet wakefulness. Similarly, during NREM sleep, fluctuations of the SWA were more strongly synchronized between somatosensory and motor areas and between associative and higher -order areas (PtA, mPFC, and dCA1) but were otherwise poorly correlated. Finally, we used coherence analysis to investigate the state-dependent changes in synchronization of cortical activities between areas. Surprisingly, we found that NREM sleep, which is characterized by strong and generalized LF activities across all cortical areas, showed poor long-range synchrony between areas in this frequency band. In contrast, the smaller amplitude LF activities during wakefulness showed high long-range synchrony. The change in long-range synchrony in the LF domain could thus reflect a change in functional coupling and cortical integration correlated to different states of arousal or consciousness.

Technical Considerations

In our study, LFP recordings have been performed in head-fixed mice to reduce movement artifacts that can be particularly problematic when recording with high-impedance electrodes in freely moving mice. To estimate a possible contamination of the LFP recordings by EMG or movement artifacts, we performed broadband LFP and EMG recordings and computed the coherence between LFPs and EMG. We found that EMG or movement activity had minimal impact on our LFP recordings between 1 and 70 Hz and only moderate impact below 1 Hz or above 70 Hz (see Supplementary Fig. 5), indicating that the contamination of the LFPs by EMG or movement artifacts is minimal in the frequency domain of interest in our study, and cannot explain the observed state-dependent changes in interareal coherence. It should be mentioned also that during quiet wakefulness, the mice are immobile and the EMG activity is low; therefore, movement artifacts or EMG contamination cannot account for the marked changes in LFP activity and coherence observed from quiet wakefulness to NREM sleep.

However, one may expect that restraining the movements of the mouse may significantly impact the overall cortical dynamics. Yet, recent studies performed in different cortical areas have shown that the cortical dynamic during quiet wakefulness (i.e., high-amplitude LF activities) and state change during active wakefulness that we report in our study are preserved in head-fixed mice running on a treadmill (Niell and Stryker 2010; Bennett et al. 2013; Polack et al. 2013; Reimer et al. 2014; Schneider et al. 2014; Zhou et al. 2014) or even in freely moving mice (Schneider et al. 2014). In head-restrained mice, the strongest impact on the cortical activity and interareal synchronization appears to be due to the behavioral context rather than the restriction of head-movements (Sachidhanandam et al. 2013; Chen et al. 2016). The interareal coherence could be stronger in animals navigating freely in their environment and/or engaged in a task. Indeed, strong synchronizations of neuronal activity have been reported between the mPFC and hippocampus (Benchenane et al. 2010; Fujisawa and Buzsaki 2011; Place et al. 2016) or the primary somatosensory cortex and the hippocampus (Grion et al. 2016) in freely moving rodents engaged in a task for instance. Therefore, our findings regarding the state change during the transition from quiet to active wakefulness and changes in coherence between wakefulness and NREM sleep should not be drastically affected by our recording conditions. Yet, it would be important in future studies to investigate long-range interareal synchronization in mice involved in a task or during subsequent sleep (Miyamoto et al. 2016).

LF Cortical Activities

Cortical LF activities, and especially in the slow (0.25–2 Hz) and delta (2–5 Hz) frequency bands, have long been associated with states of NREM sleep and anesthesia. LF activities are mainly cortically generated (Sanchez-Vives and McCormick 2000; Timofeev et al. 2000) and initiate in the infragranular layers of the cortex from where they propagate vertically to the entire column and laterally to neighboring columns (Sakata and Harris 2009; Chauvette et al. 2010; Beltramo et al. 2013; Stroh et al. 2013; Zhao et al. 2016). Recent studies from ours and other teams have consistently reported high-amplitude LF (<10 Hz) activities during quiet wakefulness in different cortical areas of rodents, including somatosensory and motor areas (Crochet and Petersen 2006; Sobolewski et al. 2011; Zagha et al. 2013), primary auditory and visual areas (Bennett et al. 2013; Polack et al. 2013; Reimer et al. 2014; Schneider et al. 2014; Zhou et al. 2014), as well as parietal and prefrontal areas (Okun et al. 2010; Fujisawa and Buzsaki 2011; Vyazovskiy et al. 2011; Parker et al. 2014). However, regional differences regarding the expression of LF activities during quiet wakefulness can be found in previous studies. LF activities seem more prominent during quiet wakefulness in somatosensory areas (Crochet and Petersen 2006; Sobolewski et al. 2011; Zagha et al. 2013) than in visual cortex (Bennett et al. 2013; Haider et al. 2013; Polack et al. 2013; Reimer et al. 2014). In the auditory cortex, LF activities have also been reported consistently in some studies (Schneider et al. 2014; Zhou et al. 2014), but with more variability across neurons in another study (Hromadka et al. 2013). The regional differences found in previous studies could reflect areas specificities but could also be attributed to different experimental conditions across studies. To resolve this issue, we have recorded from different cortical areas simultaneously in the same mice and same experimental conditions. We indeed found regional differences in the expression of LF activities during quiet wakefulness, with strongest expression in the somatosensory and motor areas and lowest expression in the auditory and parietal areas. LF activities in sensory, motor, and parietal areas appeared as broadband irregular activities in contrast with the narrow-band oscillatory activity recorded in the mPFC. The different expressions of LF activities across cortical areas could result from different intrinsic properties of the neurons in given areas or different local connectivity.

Our study also confirms a prominent LF oscillation in mPFC with a clear peak between 2 and 6 Hz, similar to what have been described in freely moving rats (Fujisawa and Buzsaki 2011). Interestingly, the LF oscillation in the mPFC often persisted during active wakefulness with a slight shift in the peak frequency toward 6 Hz. During short periods of very active behavior, we occasionally observed simultaneous theta oscillations in the hippocampus and the mPFC (see Supplementary Fig. 4). Strong coupling of activity between the mPFC and the ventral hippocampus in the theta frequency band has been observed in rodents performing different behavioral tasks (Adhikari et al. 2010; Benchenane et al. 2010; Popa et al. 2010). In contrast with these studies, we recorded from the dorsal part of the hippocampus, which does not project directly to mPFC, and the mice were not engaged in any behavioral task and could not navigate in their environment. It is thus possible

that stronger coherence between mPFC and dCA1 would be observed in mice navigating and/or performing a behavioral task.

The cortical activity observed during quiet wakefulness differed markedly from that of NREM sleep: we observed a further increase in LF activities in all cortical areas compared with quiet wakefulness, especially in the lowest frequency bands (<5 Hz) with a prominent peak around 1 Hz, reflecting the characteristic SWA (or slow oscillation) of NREM sleep (Steriade et al. 1993b; Achermann and Borbely 1997; Steriade and Amzica 1998). We also observed an increase in the 10–15 Hz frequency band (see Fig. 3A and see Supplementary Fig. 7), reflecting sleep spindle activity (Contreras et al. 1997; Steriade and Amzica 1998; Huguenard and McCormick 2007). Interestingly, we also found regional differences in the expression of LF activities during NREM sleep, similar to what has been recently reported during natural NREM sleep in the cat (Chauvette et al. 2011). However, the amplitude of LF activity within NREM sleep episodes appeared more homogeneous than that of wakefulness in most cortical areas, suggesting a relatively homogenous brain state, compared with wakefulness.

There is clear evidence from previous studies that sensory areas undergo a major state change during transitions from quiet to active wakefulness with strong decrease in LF activities and reduction in membrane potential fluctuations (Crochet and Petersen 2006; Gentet et al. 2010; Bennett et al. 2013; Polack et al. 2013; Zagha et al. 2013; Reimer et al. 2014; Schneider et al. 2014; Zhou et al. 2014; McGinley et al. 2015a). This state change could result from the simultaneous activation of thalamocortical inputs, cholinergic and/or noradrenergic inputs (Constantinople and Bruno 2011; Poulet et al. 2012; Pinto et al. 2013; Polack et al. 2013; Eggermann et al. 2014; Chen et al. 2015; Nelson and Mooney 2016), as well as long-range cortical inputs from frontal areas (Zagha et al. 2013; Schneider et al. 2014; Zhang et al. 2014; Nelson and Mooney 2016). Our data generally confirm the state change occurring during transitions from quiet to active wakefulness in most cortical areas with, on average, a prominent decrease in LF activities during active wakefulness, compared with quiet wakefulness. We also observed that activated cortical states (i.e., low LF/HF ratio) could occur during quiet wakefulness (Sobolewski et al. 2011; Reimer et al. 2014; Urbain et al. 2015; McGinley et al. 2015a). Cortical activation during quiet wakefulness may reflect transitory periods of increased arousal, attention, or sensory processing (Vinck et al. 2015; McGinley et al. 2015a, 2015b). In good agreement with a previous study in rats (Vyazovskiy et al. 2011), we found that epochs of cortical activation or deactivation could sometime occur at a more local scale, resulting in temporary desynchronized cortical states across areas (see Fig. 4A). Thus, multisite LFP recordings during wakefulness in the mouse reveal a much more complex spatiotemporal organization of cortical activation than EEG recordings. These results suggest that different parallel pathways are able to activate the cortex, either globally or more locally, depending on behavioral and environmental contexts (Lewis et al. 2015; Kim et al. 2016; Nelson and Mooney 2016). It would be interesting in future studies to record simultaneously from thalamic nuclei of different modalities to assess whether the activity of thalamocortical neurons could be differentially modulated and explain uncorrelated regional activation at cortical level (Poulet et al. 2012; Lewis et al. 2015; Urbain et al. 2015). Top-down activation from frontal areas may also impact on cortical states with regional specificity (Zagha et al. 2013; Schneider et al. 2014; Zhang et al. 2014).

Long-Range Synchrony in the LF Band

Functional coupling between distributed cortical areas through synchronized activities is supposed to play an important role for many cognitive processes, including sensory perception, attention, decision-making (Varela et al. 2001; Buzsaki and Draguhn 2004), and support consciousness (Tononi and Massimini 2008; Boly et al. 2012). Historically, wakefulness has been described as a state of HF and desynchronized cortical activity as opposed to NREM sleep described as a state of LF and synchronized cortical activity. However, latter-on, long-range synchrony in the HF band was found to be particularly prominent during wakefulness (Steriade et al. 1996; Destexhe et al. 1999) and especially during different cognitive processes, such as perception or attention (Jensen et al. 2007; Melloni et al. 2007). In fact, long-range interareal correlation or coherence in the gamma frequency band has been found to be higher during wakefulness than during NREM sleep or anesthesia (Destexhe et al. 1999; Cantero et al. 2004; Del Cul et al. 2007; Hwang et al. 2013). In this study, we confirmed these findings and found that the coherence between areas showed a clear peak in the gamma frequency band (around 60 Hz) during both active and quiet wakefulness that disappeared during NREM sleep.

Contrary to HF activities, long-range synchronization in the LF range was expected to be the highest during NREM sleep, due to the widespread expression of SWA across cortical areas (Amzica and Steriade 1995; Isomura et al. 2006; Volgushev et al. 2006; Busche et al. 2015). However, it should be noted that the long-range coherence of slow cortical activities is reduced during NREM sleep compared with anesthetized animals (Chauvette et al. 2011; Busche et al. 2015). In fact, during NREM sleep, cortical slow-waves occur mostly locally (Nir et al. 2011) and propagate to other cortical areas following variable directions (Massimini et al. 2004). Thus, the relative phase of the slow-waves may vary across cortical areas and from cycle to cycle, resulting in an overall decrease in the long-range coherence and a functional uncoupling between distant cortical areas. In good agreement, an early study in humans has found that the coherence of EEG signals recorded during NREM sleep was high in the LF range between homologous interhemispheric derivations, but was low for intrahemispheric and nonhomologous interhemispheric derivations (Achermann and Borbely 1998). In our study, we have found low coherence of LFPs in the LF range during NREM sleep between areas from the same hemisphere that are not directly synaptically connected, whereas the coherence between S1, S2, and M1—that are densely and reciprocally connected (Aronoff et al. 2010; Zingg et al. 2014; Suter and Shepherd 2015)—remained high during NREM sleep. This finding is in good agreement with a recent study in rat showing a decrease in functional coupling between excitatory neurons from distant areas during NREM sleep compared with wakefulness (Olcese et al. 2016). Our findings are also very consistent with other studies showing a marked decrease of the functional connectivity between cortical areas associated with loss of consciousness during NREM sleep or anesthesia (Massimini et al. 2005; Ferrarelli et al. 2010; Lewis et al. 2012; Bettinardi et al. 2015). However, synchronized SWA between synaptically connected areas during NREM sleep may enable synaptic plasticity required for the formation of memory traces of information acquired during preceding wakefulness (Chauvette et al. 2012; Miyamoto et al. 2016).

Because LF cortical activities are the hallmark of NREM sleep and anesthesia, the long-range cortical synchronization in the LF band during wakefulness and cognitive processes has been little studied. Recent studies, however, have pointed to

important synchronization between cortical areas, in particular the prefrontal cortex and the hippocampus in the low-frequency bands during behavioral tasks in monkeys and rats (Fujisawa and Buzsaki 2011; Nacher et al. 2013; Grion et al. 2016). These recent studies suggest that important functional coupling between cortical areas may also occur in the LF domain during wakefulness. Importantly, because LF activities have higher energy and allow integration of neuronal activity on longer time scale, they might be more efficient in terms of information transfer than faster oscillations. Thus, the high synchrony of LF activities observed during wakefulness may support higher cortical integration necessary for cognitive processes.

Conclusions

All together our data support the idea that during NREM sleep, cortical deafferentation from thalamus and ascending neuromodulators leads to the generation of locally synchronized LF activities (Chauvette et al. 2010) with strong coupling between synaptically connected cortical neurons (Esser et al. 2007). Because slow oscillations can be generated locally at any cortical site and propagate to other cortical areas in any direction (Massimini et al. 2004), distant cortical sites that are not directly synaptically coupled would often be out of phase thereby preventing efficient propagation of information across cortical areas (Massimini et al. 2005). This is reflected by the low coherence in the LF band between cortical areas that are not directly connected. Therefore, NREM sleep is associated with high amplitude, LF activities with high local, but poor long-range synchrony (Olcese et al. 2016). In contrast, wakefulness is associated with smaller amplitude LF activities with lower local (Poulet and Petersen 2008), but higher long-range, synchrony (Olcese et al. 2016). This long-range synchrony of LF activities may reflect a state of high functional coupling and integration between cortical areas. It is particularly interesting to note that the highest coherence observed during wakefulness involved particularly the parietal and prefrontal areas (PtA and mPFC). In good agreement with previous functional connectivity studies, our results suggest that these 2 cortical regions could be important cortical hubs (Honey et al. 2007; Buckner et al. 2009; Lim et al. 2012). Through highly synchronized activity across distant cortical areas, PtA and mPFC may play an important role for attentional processes, multimodal sensory integration and memory. In good agreement, we found that the correlation between these 2 areas and with other cortical areas increased during active behavior, as compared with quiet wakefulness. In future studies, it would be of great interest to investigate long-range cortical synchronization in mice engaged in behavioral tasks.

Supplementary Material

Supplementary material can be found at: http://www.cercor.oxfordjournals.org/

Funding

Institut National de la Santé et de la Recherche Médicale (INSERM) and University Claude Bernard—Lyon 1 and Agence Nationale de la Recherche (Project AWAKE CX, ANR-09-JCJC-0028-01, 2009); Lyon Neuroscience Research Center (Projet Structurant, 2009); the European Community, Fifth Framework Program (Grant QLRT-2001-00826, 2001). Fondation pour la Recherche Médicale (FRM Fin de Thèse, 2011 to L.M.J.F.).

Notes

We thank C. Buda, M. Perier, and N. Clairis for technical assistance and help with the experiments. We thank C. Petersen and J. Poulet for discussion and critical reading of the manuscript. *Conflict of Interest:* None declared.

References

Achermann P, Borbely AA. 1997. Low-frequency (<1 Hz) oscillations in the human sleep electroencephalogram. Neuroscience. 81:213–222.

Achermann P, Borbely AA. 1998. Coherence analysis of the human sleep electroencephalogram. Neuroscience. 85: 1195–1208.

Adhikari A, Topiwala MA, Gordon JA. 2010. Synchronized activity between the ventral hippocampus and the medial prefrontal cortex during anxiety. Neuron. 65:257–269.

Aeschbach D, Borbely AA. 1993. All-night dynamics of the human sleep EEG. J Sleep Res. 2:70–81.

Amzica F, Steriade M. 1995. Short- and long-range neuronal synchronization of the slow (<1 Hz) cortical oscillation. J Neurophysiol. 73:20–38.

Aronoff R, Matyas F, Mateo C, Ciron C, Schneider B, Petersen CC. 2010. Long-range connectivity of mouse primary somatosensory barrel cortex. Eur J Neurosci. 31:2221–2233.

Beltramo R, D'Urso G, Dal Maschio M, Farisello P, Bovetti S, Clovis Y, Lassi G, Tucci V, De Pietri Tonelli D, Fellin T. 2013. Layer-specific excitatory circuits differentially control recurrent network dynamics in the neocortex. Nat Neurosci. 16: 227–234.

Benchenane K, Peyrache A, Khamassi M, Tierney PL, Gioanni Y, Battaglia FP, Wiener SI. 2010. Coherent theta oscillations and reorganization of spike timing in the hippocampal- prefrontal network upon learning. Neuron. 66:921–936.

Bennett C, Arroyo S, Hestrin S. 2013. Subthreshold mechanisms underlying state-dependent modulation of visual responses. Neuron. 80:350–357.

Berger H. 1929. Ueber das Elektroenkephalogramm des Menschen. Arch Psychiatr Nervenkrankh. 87:527–570.

Bettinardi RG, Tort-Colet N, Ruiz-Mejias M, Sanchez-Vives MV, Deco G. 2015. Gradual emergence of spontaneous correlated brain activity during fading of general anesthesia in rats: evidences from fMRI and local field potentials. Neuroimage. 114:185–198.

Boly M, Perlbarg V, Marrelec G, Schabus M, Laureys S, Doyon J, Pelegrini-Issac M, Maquet P, Benali H. 2012. Hierarchical clustering of brain activity during human nonrapid eye movement sleep. Proc Natl Acad Sci U S A. 109:5856–5861.

Brown RE, Basheer R, McKenna JT, Strecker RE, McCarley RW. 2012. Control of sleep and wakefulness. Physiol Rev. 92: 1087–1187.

Buckner RL, Sepulcre J, Talukdar T, Krienen FM, Liu H, Hedden T, Andrews-Hanna JR, Sperling RA, Johnson KA. 2009. Cortical hubs revealed by intrinsic functional connectivity: mapping, assessment of stability, and relation to Alzheimer's disease. J Neurosci. 29:1860–1873.

Busche MA, Kekus M, Adelsberger H, Noda T, Forstl H, Nelken I, Konnerth A. 2015. Rescue of long-range circuit dysfunction in Alzheimer's disease models. Nat Neurosci. 18:1623–1630.

Buzsaki G, Draguhn A. 2004. Neuronal oscillations in cortical networks. Science. 304:1926–1929.

Cantero JL, Atienza M, Madsen JR, Stickgold R. 2004. Gamma EEG dynamics in neocortex and hippocampus during human wakefulness and sleep. Neuroimage. 22:1271–1280.

Chauvette S, Crochet S, Volgushev M, Timofeev I. 2011. Properties of slow oscillation during slow-wave sleep and anesthesia in cats. J Neurosci. 31:14998–15008.

Chauvette S, Seigneur J, Timofeev I. 2012. Sleep oscillations in the thalamocortical system induce long-term neuronal plasticity. Neuron. 75:1105–1113.

Chauvette S, Volgushev M, Timofeev I. 2010. Origin of active states in local neocortical networks during slow sleep oscillation. Cereb Cortex. 20:2660–2674.

Chen JL, Voigt FF, Javadzadeh M, Krueppel R, Helmchen F. 2016. Long-range population dynamics of anatomically defined neocortical networks. Elife. 5:e14679.

Chen N, Sugihara H, Sur M. 2015. An acetylcholine-activated microcircuit drives temporal dynamics of cortical activity. Nat Neurosci. 18:892–902.

Constantinople CM, Bruno RM. 2011. Effects and mechanisms of wakefulness on local cortical networks. Neuron. 69:1061–1068.

Contreras D, Destexhe A, Sejnowski TJ, Steriade M. 1997. Spatiotemporal patterns of spindle oscillations in cortex and thalamus. J Neurosci. 17:1179–1196.

Crochet S. 2012.Intracellular whole-cell patch-clamp recordings of cortical neurons in awake head-restrained mice. In: Fellin T, Halassa M, editors.Neural Network Analysis. New York: Humana Press. p. 219–235.

Crochet S, Petersen CC. 2006. Correlating whisker behavior with membrane potential in barrel cortex of awake mice. Nat Neurosci. 9:608–610.

Del Cul A, Baillet S, Dehaene S. 2007. Brain dynamics underlying the nonlinear threshold for access to consciousness. PLoS Biol. 5:e260.

Destexhe A, Contreras D, Steriade M. 1999. Spatiotemporal analysis of local field potentials and unit discharges in cat cerebral cortex during natural wake and sleep states. J Neurosci. 19:4595–4608.

Eggermann E, Kremer Y, Crochet S, Petersen CC. 2014. Cholinergic signals in mouse barrel cortex during active whisker sensing. Cell Rep. 9:1654–1660.

Esser SK, Hill SL, Tononi G. 2007. Sleep homeostasis and cortical synchronization: I. Modeling the effects of synaptic strength on sleep slow waves. Sleep. 30:1617–1630.

Ferrarelli F, Massimini M, Sarasso S, Casali A, Riedner BA, Angelini G, Tononi G, Pearce RA. 2010. Breakdown in cortical effective connectivity during midazolam-induced loss of consciousness. Proc Natl Acad Sci U S A. 107:2681–2686.

Franken P, Malafosse A, Tafti M. 1998. Genetic variation in EEG activity during sleep in inbred mice. Am J Physiol. 275: R1127–R1137.

Fujisawa S, Buzsaki G. 2011. A 4 Hz oscillation adaptively synchronizes prefrontal, VTA, and hippocampal activities. Neuron. 72:153–165.

Gentet LJ, Avermann M, Matyas F, Staiger JF, Petersen CC. 2010. Membrane potential dynamics of GABAergic neurons in the barrel cortex of behaving mice. Neuron. 65:422–435.

Gervasoni D, Lin SC, Ribeiro S, Soares ES, Pantoja J, Nicolelis MA. 2004. Global forebrain dynamics predict rat behavioral states and their transitions. J Neurosci. 24: 11137–11147.

Grion N, Akrami A, Zuo Y, Stella F, Diamond ME. 2016. Coherence between rat sensorimotor system and hippocampus is enhanced during tactile discrimination. PLoS biology. 14:e1002384.

Haider B, Hausser M, Carandini M. 2013. Inhibition dominates sensory responses in the awake cortex. Nature. 493:97–100.

Hobson JA, Pace-Schott EF. 2002. The cognitive neuroscience of sleep: neuronal systems, consciousness and learning. Nat Rev Neurosci. 3:679–693.

Honey CJ, Kotter R, Breakspear M, Sporns O. 2007. Network structure of cerebral cortex shapes functional connectivity on multiple time scales. Proc Natl Acad Sci U S A. 104: 10240–10245.

Hromadka T, Zador AM, DeWeese MR. 2013. Up states are rare in awake auditory cortex. J Neurophysiol. 109:1989–1995.

Huguenard JR, McCormick DA. 2007. Thalamic synchrony and dynamic regulation of global forebrain oscillations. Trends Neurosci. 30:350–356.

Hwang E, McNally JM, Choi JH. 2013. Reduction in cortical gamma synchrony during depolarized state of slow wave activity in mice. Front Syst Neurosci. 7:107.

Isomura Y, Sirota A, Ozen S, Montgomery S, Mizuseki K, Henze DA, Buzsaki G. 2006. Integration and segregation of activity in entorhinal-hippocampal subregions by neocortical slow oscillations. Neuron. 52:871–882.

Jensen O, Kaiser J, Lachaux JP. 2007. Human gamma-frequency oscillations associated with attention and memory. Trends Neurosci. 30:317–324.

Jones BE. 2005. From waking to sleeping: neuronal and chemical substrates. Trends Pharmacol Sci. 26:578–586.

Jouvet M. 1967. Neurophysiology of the states of sleep. Physiol Rev. 47:117–177.

Karalis N, Dejean C, Chaudun F, Khoder S, Rozeske RR, Wurtz H, Bagur S, Benchenane K, Sirota A, Courtin J, et al. 2016. 4-Hz oscillations synchronize prefrontal-amygdala circuits during fear behavior. Nat Neurosci. 19:605–612.

Kim JH, Jung AH, Jeong D, Choi I, Kim K, Shin S, Kim SJ, Lee SH. 2016. Selectivity of neuromodulatory projections from the basal forebrain and locus ceruleus to primary sensory cortices. J Neurosci. 36:5314–5327.

Le Van Quyen M, Staba R, Bragin A, Dickson C, Valderrama M, Fried I, Engel J. 2010. Large-scale microelectrode recordings of high-frequency gamma oscillations in human cortex during sleep. J Neurosci. 30:7770–7782.

Lewis LD, Voigts J, Flores FJ, Schmitt LI, Wilson MA, Halassa MM, Brown EN. 2015. Thalamic reticular nucleus induces fast and local modulation of arousal state. Elife. 4:e08760.

Lewis LD, Weiner VS, Mukamel EA, Donoghue JA, Eskandar EN, Madsen JR, Anderson WS, Hochberg LR, Cash SS, Brown EN, et al. 2012. Rapid fragmentation of neuronal networks at the onset of propofol-induced unconsciousness. Proc Natl Acad Sci U S A. 109:E3377–3386.

Lim DH, Mohajerani MH, Ledue J, Boyd J, Chen S, Murphy TH. 2012. In vivo large-scale cortical mapping using channelrhodopsin-2 stimulation in transgenic mice reveals asymmetric and reciprocal relationships between cortical areas. Front Neural Circuits. 6:11.

Lin JS. 2000. Brain structures and mechanisms involved in the control of cortical activation and wakefulness, with emphasis on the posterior hypothalamus and histaminergic neurons. Sleep Med Rev. 4:471–503.

Loomis AL, Harvey EN, Hobart G. 1935. Further observations on the potential rhythms of the cerebral cortex during sleep. Science. 82:198–200.

Maloney KJ, Cape EG, Gotman J, Jones BE. 1997. High-frequency gamma electroencephalogram activity in association with sleep-wake states and spontaneous behaviors in the rat. Neuroscience. 76:541–555.

Massimini M, Ferrarelli F, Huber R, Esser SK, Singh H, Tononi G. 2005. Breakdown of cortical effective connectivity during sleep. Science. 309:2228–2232.

Massimini M, Huber R, Ferrarelli F, Hill S, Tononi G. 2004. The sleep slow oscillation as a traveling wave. J Neurosci. 24: 6862–6870.

McGinley MJ, David SV, McCormick DA. 2015a. Cortical membrane potential signature of optimal states for sensory signal detection. Neuron. 87:179–192.

McGinley MJ, Vinck M, Reimer J, Batista-Brito R, Zagha E, Cadwell CR, Tolias AS, Cardin JA, McCormick DA. 2015b. Waking state: rapid variations modulate neural and behavioral responses. Neuron. 87:1143–1161.

Melloni L, Molina C, Pena M, Torres D, Singer W, Rodriguez E. 2007. Synchronization of neural activity across cortical areas correlates with conscious perception. J Neurosci. 27: 2858–2865.

Mena-Segovia J, Sims HM, Magill PJ, Bolam JP. 2008. Cholinergic brainstem neurons modulate cortical gamma activity during slow oscillations. J Physiol. 586:2947–2960.

Miyamoto D, Hirai D, Fung CC, Inutsuka A, Odagawa M, Suzuki T, Boehringer R, Adaikkan C, Matsubara C, Matsuki N, et al. 2016. Top-down cortical input during NREM sleep consolidates perceptual memory. Science. 352:1315–1318.

Moruzzi G, Magoun HW. 1949. Brainstem reticular formation and activation of the EEG. EEG and Clin Neurophysiol. 1: 455–473.

Mukovski M, Chauvette S, Timofeev I, Volgushev M. 2007. Detection of active and silent states in neocortical neurons from the field potential signal during slow-wave sleep. Cereb cortex. 17:400–414.

Nacher V, Ledberg A, Deco G, Romo R. 2013. Coherent delta-band oscillations between cortical areas correlate with decision making. Proc Natl Acad Sci U S A. 110:15085–15090.

Nelson A, Mooney R. 2016. The basal forebrain and motor cortex provide convergent yet distinct movement-related inputs to the auditory cortex. Neuron. 90:635–648.

Niell CM, Stryker MP. 2010. Modulation of visual responses by behavioral state in mouse visual cortex. Neuron. 65:472–479.

Nir Y, Staba RJ, Andrillon T, Vyazovskiy VV, Cirelli C, Fried I, Tononi G. 2011. Regional slow waves and spindles in human sleep. Neuron. 70:153–169.

Okun M, Naim A, Lampl I. 2010. The subthreshold relation between cortical local field potential and neuronal firing unveiled by intracellular recordings in awake rats. J Neurosci. 30:4440–4448.

Olcese U, Bos JJ, Vinck M, Lankelma JV, van Mourik-Donga LB, Schlumm F, Pennartz CM. 2016. Spike-based functional connectivity in cerebral cortex and hippocampus: loss of global connectivity is coupled to preservation of local connectivity during non-rem sleep. J Neurosci. 36:7676–7692.

Parker KL, Chen KH, Kingyon JR, Cavanagh JF, Narayanan NS. 2014. D1-dependent 4 Hz oscillations and ramping activity in rodent medial frontal cortex during interval timing. J Neurosci. 34:16774–16783.

Parmentier R, Ohtsu H, Djebbara-Hannas Z, Valatx JL, Watanabe T, Lin JS. 2002. Anatomical, physiological, and pharmacological characteristics of histidine decarboxylase knock-out mice: evidence for the role of brain histamine in behavioral and sleep-wake control. J Neurosci. 22:7695–7711.

Paxinos G, Franklin KBJ. 2008.The mouse brain in stereotaxic coordinates. 3rd ed. Oxford (Oxford): Elsevier.

Pinto L, Goard MJ, Estandian D, Xu M, Kwan AC, Lee SH, Harrison TC, Feng G, Dan Y. 2013. Fast modulation of visual perception by basal forebrain cholinergic neurons. Nat Neurosci. 16:1857–1863.

Place R, Farovik A, Brockmann M, Eichenbaum H. 2016. Bidirectional prefrontal-hippocampal interactions support context-guided memory. Nat Neurosci. 19:992–994.

Polack PO, Friedman J, Golshani P. 2013. Cellular mechanisms of brain state-dependent gain modulation in visual cortex. Nat Neurosci. 16:1331–1339.

Popa D, Duvarci S, Popescu AT, Lena C, Pare D. 2010. Coherent amygdalocortical theta promotes fear memory consolidation during paradoxical sleep. Proc Natl Acad Sci U S A. 107: 6516–6519.

Poulet JF, Fernandez LM, Crochet S, Petersen CC. 2012. Thalamic control of cortical states. Nat Neurosci. 15:370–372.

Poulet JF, Petersen CC. 2008. Internal brain state regulates membrane potential synchrony in barrel cortex of behaving mice. Nature. 454:881–885.

Reimer J, Froudarakis E, Cadwell CR, Yatsenko D, Denfield GH, Tolias AS. 2014. Pupil fluctuations track fast switching of cortical states during quiet wakefulness. Neuron. 84: 355–362.

Rheinberger M, Jasper HH. 1937. Electrical activity of the cerebral cortex in the unanesthetized cat. Am J Physiol. 119: 186–196.

Sachidhanandam S, Sreenivasan V, Kyriakatos A, Kremer Y, Petersen CC. 2013. Membrane potential correlates of sensory perception in mouse barrel cortex. Nat Neurosci. 16: 1671–1677.

Sakata S, Harris KD. 2009. Laminar structure of spontaneous and sensory-evoked population activity in auditory cortex. Neuron. 64:404–418.

Sanchez-Vives MV, McCormick DA. 2000. Cellular and network mechanisms of rhythmic recurrent activity in neocortex. Nat Neurosci. 3:1027–1034.

Schneider DM, Nelson A, Mooney R. 2014. A synaptic and circuit basis for corollary discharge in the auditory cortex. Nature. 513:189–194.

Sirota A, Montgomery S, Fujisawa S, Isomura Y, Zugaro M, Buzsaki G. 2008. Entrainment of neocortical neurons and gamma oscillations by the hippocampal theta rhythm. Neuron. 60:683–697.

Sobolewski A, Swiejkowski DA, Wrobel A, Kublik E. 2011. The 5-12 Hz oscillations in the barrel cortex of awake rats–sustained attention during behavioral idling? Clin Neurophysiol. 122:483–489.

Steriade M. 2000. Corticothalamic resonance, states of vigilance and mentation. Neuroscience. 101:243–276.

Steriade M, Amzica F. 1998. Coalescence of sleep rhythms and their chronology in corticothalamic networks. Sleep Res Online. 1:1–10.

Steriade M, Amzica F, Contreras D. 1996. Synchronization of fast (30–40 Hz) spontaneous cortical rhythms during brain activation. J Neurosci. 16:392–417.

Steriade M, Dossi RC, Nunez A. 1991. Network modulation of a slow intrinsic oscillation of cat thalamocortical neurons implicated in sleep delta waves: cortically induced synchronization and brainstem cholinergic suppression. J Neurosci. 11:3200–3217.

Steriade M, McCormick DA, Sejnowski TJ. 1993a. Thalamocortical oscillations in the sleeping and aroused brain. Science. 262:679–685.

Steriade M, Nunez A, Amzica F. 1993b. A novel slow (<1 Hz) oscillation of neocortical neurons in vivo: depolarizing and hyperpolarizing components. J Neurosci. 13:3252–3265.

Stroh A, Adelsberger H, Groh A, Ruhlmann C, Fischer S, Schierloh A, Deisseroth K, Konnerth A. 2013. Making waves: initiation and propagation of corticothalamic ca(2+) waves in vivo. Neuron. 77:1136–1150.

Suter BA, Shepherd GM. 2015. Reciprocal interareal connections to corticospinal neurons in mouse m1 and s2. J Neurosci. 35: 2959–2974.

Takahashi K, Lin JS, Sakai K. 2006. Neuronal activity of histaminergic tuberomammillary neurons during wake-sleep states in the mouse. J Neurosci. 26:10292–10298.

Timofeev I, Grenier F, Bazhenov M, Sejnowski TJ, Steriade M. 2000. Origin of slow cortical oscillations in deafferented cortical slabs. Cereb Cortex. 10:1185–1199.

Tononi G, Massimini M. 2008. Why does consciousness fade in early sleep? Ann N Y Acad Sci. 1129:330–334.

Urbain N, Salin PA, Libourel PA, Comte JC, Gentet LJ, Petersen CC. 2015. Whisking-related changes in neuronal firing and membrane potential dynamics in the somatosensory thalamus of awake mice. Cell Rep. 13:647–656.

Valatx JL. 1971. Enregistrement chronique des activités électriques cérébrales musculaires et oculaires chez la souris. C R Seances Soc Biol Fil. 165:112–115.

Varela F, Lachaux JP, Rodriguez E, Martinerie J. 2001. The brainweb: phase synchronization and large-scale integration. Nat Rev Neurosci. 2:229–239.

Vinck M, Batista-Brito R, Knoblich U, Cardin JA. 2015. Arousal and locomotion make distinct contributions to cortical activity patterns and visual encoding. Neuron. 86:740–754.

Volgushev M, Chauvette S, Mukovski M, Timofeev I. 2006. Precise long-range synchronization of activity and silence in neocortical neurons during slow-wave oscillations. J Neurosci. 26:5665–5672.

Vyazovskiy VV, Olcese U, Hanlon EC, Nir Y, Cirelli C, Tononi G. 2011. Local sleep in awake rats. Nature. 472:443–447.

Zagha E, Casale AE, Sachdev RN, McGinley MJ, McCormick DA. 2013. Motor cortex feedback influences sensory processing by modulating network state. Neuron. 79:567–578.

Zhang S, Xu M, Kamigaki T, Hoang Do JP, Chang WC, Jenvay S, Miyamichi K, Luo L, Dan Y. 2014. Selective attention. Long-range and local circuits for top-down modulation of visual cortex processing. Science. 345:660–665.

Zhao WJ, Kremkow J, Poulet JF. 2016. Translaminar cortical membrane potential synchrony in behaving mice. Cell Rep. 15:2387–2399.

Zhou M, Liang F, Xiong XR, Li L, Li H, Xiao Z, Tao HW, Zhang LI. 2014. Scaling down of balanced excitation and inhibition by active behavioral states in auditory cortex. Nat Neurosci. 17:841–850.

Zingg B, Hintiryan H, Gou L, Song MY, Bay M, Bienkowski MS, Foster NN, Yamashita S, Bowman I, Toga AW, et al. 2014. Neural networks of the mouse neocortex. Cell. 156:1096–1111.